# The actin binding protein $\alpha$-actinin-2 expression is associated with dendritic spine plasticity and migrating granule cells in the rat dentate gyrus following pilocarpine-induced seizures

Oualid Sbai, Rabia Soussi, Angélique Bole, Michel Khrestchatisky, Monique Esclapez, Lotfi Ferhat

Experimental Neurology 335 (2021) 113512

Contents lists available at ScienceDirect

Experimental Neurology

journal homepage: www.elsevier.com/locate/yexnr

Research paper

# The actin binding protein α-actinin-2 expression is associated with dendritic spine plasticity and migrating granule cells in the rat dentate gyrus following pilocarpine-induced seizures

Oualid Sbai [a], Rabia Soussi [a], Angélique Bole [a], Michel Khrestchatisky [a], Monique Esclapez [b], Lotfi Ferhat [a,*]

[a] Aix-Marseille Univ, CNRS, INP, Inst Neurophysiopathol, Marseille, France
[b] Aix-Marseille Univ, INSERM, INS, Inst Neurosci Syst, Marseille, France

ARTICLE INFO

*Keywords:*
Hippocampus
dentate gyrus
dendritic spine
spine plasticity
migrating granule cells
actin cytoskeleton
α-actinin-2

ABSTRACT

α-actinin-2 (α-actn-2) is an F-actin-crosslinking protein, localized in dendritic spines. *In vitro* studies suggested that it is involved in spinogenesis, morphogenesis, actin organization, cell migration and anchoring of the NR1 subunit of the N-methyl-D-aspartate (NMDA) receptors in dendritic spines. However, little is known regarding its function *in vivo*. We examined the levels of α-actn-2 expression within the dentate gyrus (DG) during the development of chronic limbic seizures (epileptogenesis) induced by pilocarpine in rats. In this model, plasticity of the DG glutamatergic granule cells including spine loss, spinogenesis, morphogenesis, neo-synaptogenesis, aberrant migration, and alterations of NMDA receptors have been well characterized. We showed that α-actn-2 immunolabeling was reduced in the inner molecular layer at 1-2 weeks post-status epilepticus (SE), when granule cell spinogenesis and morphogenesis occur. This low level persisted at the chronic stage when new functional synapses are established. This decreased of α-actn-2 protein is concomitant with the recovery of drebrin A (DA), another actin-binding protein, at the chronic stage. Indeed, we demonstrated in cultured cells that in contrast to DA, α-actn-2 did not protect F-actin destabilization and DA inhibited α-actn-2 binding to F-actin. Such alteration could affect the anchoring of NR1 in dendritic spines. Furthermore, we showed that the expression of α-actn-2 and NR1 are co-down-regulated in membrane fractions of pilocarpine animals at chronic stage. Last, we showed that α-actn-2 is expressed in migrating newly born granule cells observed within the hilus of pilocarpine-treated rats. Altogether, our results suggest that α-actn-2 is not critical for the structural integrity and stabilization of granule cell dendritic spines. Instead, its expression is regulated when spinogenesis and morphogenesis occur and within migrating granule cells. Our data also suggest that the balance between α-actn-2 and DA expression levels may modulate NR1 anchoring within dendritic spines.

## 1. Introduction

The actin filaments (F-actin) are the primary structural elements found in dendritic spines. Alterations in the shape and density of dendritic spines are intimately linked with regulation of actin structure and dynamics (Sekino et al., 2007; Hotulainen and Hoogenraad, 2010; Ferhat, 2012; Soria Fregozo and Pérez Vega, 2012; Lai and Ip, 2013; Bertling and Hotulainen, 2017; Koganezawa et al., 2017; Borovac et al., 2018). Therefore, the identification of the molecular bases that underlie organization and dynamics of actin filaments in dendritic spines are essential to comprehend the mechanisms of synaptic plasticity in physiological and physiopathological conditions.

α-actinins are one of the principal actin crosslinking and bundling proteins present in most cell types. They are members of the spectrin/dystrophin superfamily of proteins (Meyer and Aebi, 1990; Otey and Carpen, 2004; Sjöblom et al., 2008; Honda, 2015; Murphy and Young, 2015). Four isoforms compose the α-actinin family: α-actinin-1, -2, -3 and -4. These isoforms are encoded by four different genes (gene name; *ACTN1; ACTN2; ACTN3; ACTN4*). The mRNAs encoding α-actinin-1, -2, and -4 have been detected by RT-PCR (Schnizler et al., 2009) and the encoded proteins by mass spectrometry in post-synaptic density (PSD) preparations (Walikonis et al., 2000; Peng et al., 2004) from cultured rat

* Corresponding author.
*E-mail address:* lotfi.ferhat@univ-amu.fr (L. Ferhat).

https://doi.org/10.1016/j.expneurol.2020.113512
Received 30 June 2020; Received in revised form 8 October 2020; Accepted 19 October 2020
Available online 22 October 2020

hippocampal neurons.

Through their actin crosslinking and bundling activities, α-actinins are involved in organizing actin filaments in different cellular structures or compartments such as stress fibers (Otey and Carpen, 2004; Burridge and Wittchen, 2013), the lamellipodia of migrating cells (Small et al., 2002), and dendritic spines (Wyszynski et al., 1998; Nakagawa et al., 2004; Hodges et al., 2014). Noteworthy, these activities are inhibited by drebrin, another actin-binding protein (Ishikawa et al., 1994).

Besides its role in crosslinking and bundling actin filaments, α-actinin interacts with numerous partners (~30), including NMDA receptors, L-type calcium ($Ca^{2+}$) channel Cav1.2, potassium ($K^{+}$) channels, transient receptor potential (TRP) channels, cell adhesion proteins (e.g. integrins and cadherin), phosphatidylinositol-bisphosphate (PIP2), the α/β-catenin complex, densin-180, and Ca2+/calmodulin dependent protein kinase II alpha (CaMKIIα) (Otey et al., 1990; Pavalko et al., 1991; Otey et al., 1993; Knudsen et al., 1995; Wyszynski et al., 1997; Maruoka et al., 2000; Walikonis et al., 2001; Sadeghi et al., 2002; Otey and Carpen, 2004; Li et al., 2007; Michailidis et al., 2007; Sjöblom et al., 2008; Jalan-Sakrikar et al., 2012; Hall et al., 2013; Matt et al., 2018; Penny and Gold, 2018). As a result of these interactions, α-actinin is believed to play several important functions within the cell : it connects actin filaments to different transmembrane molecules and post-synaptic density (PSD) components, it modulates the activity of several receptors, it regulates the membrane localization, trafficking and function of cation channels and it mediates interactions between actin filaments and various signaling pathways (Wyszynski et al., 1997; Maruoka et al., 2000; Sadeghi et al., 2002; Otey and Carpen, 2004; Li et al., 2007; Sjöblom et al., 2008; Tseng et al., 2017).

Among the different actinins, immunofluorescence and immunoelectron microscopy studies revealed that α-actn-2 is highly concentrated in dendritic spines and the PSD (Wyszynski et al., 1997, 1998; Allison et al., 2000; Nakagawa et al., 2004; Hodges et al., 2014). Consistent with these localizations, several studies showed that α-actn-2 is involved in the plasticity of dendritic spines (spinogenesis, morphogenesis) and assembly of the PSD. Indeed, overexpression or down-regulation of α-actn-2 increases the density and length of dendritic protrusions that lack a PSD in cultured rat hippocampal neurons (Nakagawa et al., 2004; Hoe et al., 2009; Hodges et al., 2014). Furthermore, at resting intracellular Ca2+, α-actn-2 interacts with one component of the PSD, the NR1 subunit of the NMDA receptor (Wyszynski et al., 1997; Krupp et al., 1999; Merrill et al., 2007), suggesting that α-actn-2 functions as a post-synaptic-anchoring protein for NMDA glutamatergic receptors (Wyszynski et al., 1998).

Most of the studies on α-actn-2 regulation and function were performed using *in vitro* binding and yeast two hybrid assays or *in vitro* preparations of non-neuronal and neuronal cultures. In this study, we examined the role of α-actn-2 *in vivo,* using a pathophysiological model of temporal lobe epilepsy (TLE) induced by pilocarpine in adult rats. Indeed, this experimental model reveals extensive remodeling in the dentate gyrus, including neo-spinogenesis, morphogenesis (Isokawa and Mello, 1991; Isokawa, 1998, 2000; Kurz et al., 2008), ectopic localization of dentate granule cells (Parent et al., 1997; Covolan et al., 2000; Parent, 2002; Parent et al., 2006; Parent, 2007), and alterations of synaptic receptors such as the NMDA receptor (Geddes et al., 1990; Hosford et al., 1991; McDonald et al., 1991; Lee et al., 1994; Jiang et al., 2007; Khan et al., 2008; Di Maio et al., 2011; Lopes et al., 2013; Hoeller et al., 2016; Peng et al., 2016; Amakhin et al., 2017; Zubareva et al., 2018) following excessive glutamate release associated with long term intracellular calcium [Ca(2+)](i) (Raza et al., 2001; Costa et al., 2004; Barker-Haliski and White, 2015). At first, we investigated the regulation of α-actn-2 protein and mRNA levels at the different stages of reactive plasticity induced by pilocarpine using immunohistochemistry and *in situ* hybridization. We next evaluated its interaction with F-actin and drebrin A in cell cultures using transfection and immunocytochemistry approaches. Finally, to assess the potential role of α-actn-2 in membrane anchoring of NR1 and in dentate granule cell migration, we respectively investigated, the co-regulation of α-actn-2 and NR1 expression levels using fractionation and Western blot techniques at chronic stage as well as the expression of α-actn-2 in ectopic newly born granule cells in pilocarpine rats at latent and chronic stages.

## 2. Material and methods

### 2.1. Experimental animals

All experiments involving animals use protocols that were approved by National and European regulations (EU directive N° 2010/63) and in agreement with the authorization for animal experimentation attributed to the laboratory by the Prefecture des Bouches-du-Rhône (permit number: D 13 055 08). All efforts were made to minimize animal suffering and to reduce the number of rats used.

Adult male Wistar rats weighing 180-200 g (Charles River, France) were injected intraperitoneally (i.p.) with a low dose of the cholinergic antagonist methyl scopolamine nitrate (1 mg/kg; Sigma, Saint Louis, MO, USA), in order to minimize the peripheral effects of pilocarpine hydrochloride (340 mg/kg; Sigma), a muscarinic cholinergic agonist, provided 30 min later by i.p. injection. The injection protocols were similar to those previously described (Mello et al., 1993; Obenaus et al., 1993). In the present study, seizures were assessed by 3 different experienced observers through direct visual observation of the animals. The monitoring began on the same day (from 8 AM to 8 PM) the animals were injected and continued until their sacrifice. Fifty five to Sixty percent (55-60%) of the pilocarpine-treated animals survived the period of acute seizures (status epilepticus, SE; Esclapez et al., 1999; Goffin et al., 2007). To reduce mortality of these animals, the period of status epilepticus was stopped after 2 h by a single injection of diazepam (8 mg/kg, i.p.; Roche, Boulogne-Billancourt, France). Only animals that developed sustained SE after the pilocarpine injection were included in this study. These rats were then observed daily (at least three hours a day) in the vivarium for the occurrence of spontaneous recurrent limbic seizures (SRS). Among these animals, 90% of the pilocarpine-treated developed SRS. Only seizures of grade 3 or greater on the Racine (1972) scale were scored (i.e., forelimb clonus ± rearing ± falling). The onset of the SRS occurrence was 2-3 weeks for pilocarpine rats (Soussi et al., 2015). The frequency and intensity of seizures indeed differ from one animal to another within the same cohort, which is inherent to the model. In general, all animals display an average of 4 seizures per day in the two cohorts (one cohort used for histochemical experiments and one cohort used for biochemical analysis) used in this study, similar to that previously reported by Bajorat et al. (2011). Pilocarpine-treated animals were studied at several post-injection intervals: during the latent period, when animals displayed no behavioral seizures (1 and 2 weeks; 6 rats for each time point), and during the chronic stage, when the animals have developed SRS (8-16 weeks; 10 rats). Each group of pilocarpine-treated animals was compared to saline-treated rats used as controls. Reported histological and biochemistry observations were made of 22 pilocarpine rats and of 13 control saline-injected rats.

### 2.2. Tissue preparation

The sections used in this study for immunohistochemical and *in situ* hybridization experiments were obtained from the same rats used in a previous study (Soussi et al., 2015). Briefly, the rats were deeply anesthetized with chloral hydrate injection (500 mg/kg, i.p.) and perfused through the heart with a fixative solution of 4% paraformaldehyde (PFA). The brains were cryoprotected in a solution containing 20% sucrose, frozen on dry ice, and sectioned coronally at 40 μm with a cryostat. The sections were collected sequentially in tubes containing an ethylene glycol-based cryoprotective solution and stored at -20°C until processing.

Selected sections from each rat were processed for nonradioactive *in situ* hybridization with sense or antisense α-actn-2 cRNA probe and for

immunohistochemistry. Sections from control and pilocarpine-treated rats were always processed in parallel.

### 2.3. Immunohistochemistry

#### 2.3.1. Single immunohistochemical labeling for α-actn-2 or Prox-1

Free-floating sections were processed for immunohistochemistry with standard avidin-biotinylated-peroxidase methods (Vectastain, ABC Kit, Vector Laboratories, Burlingame, CA, USA) according to previously described protocol (Esclapez et al., 1994; Sbai et al., 2012). In this study, we used as primary antibodies, the mouse monoclonal antibody against α-actinin (1:20000; EA53, Sigma) or the rabbit antibody against Prox-1 (1/10000, Chemicon International, Temecula, CA, USA) and as secondary antibodies, the biotinylated horse anti-mouse immunoglobulin G (IgG; 1:200) or the biotinylated goat anti-rabbit IgG (1:200; Vector Laboratories, Burlingame, CA). Sections were then incubated for 1 h at RT in an avidin-biotin-peroxidase solution prepared in PB according to the manufacturer's recommendations. Then, sections from control and pilocarpine-treated rats were incubated for identical times in the chromogen solution, the 3-3-diaminobenzidine-HCl and $H_2O_2$ diluted in $dH_2O$ (Sigma fast tablets). Series of sections from all groups that were processed identically were removed from the chromogen solution at three time intervals (5, 10 and 15 min) to compare the labeling intensities among sections from the four animal groups at each interval. The differences in the levels of labeling in relation to the color-reaction times reflect differences in the amounts of proteins between groups. The sections were mounted on Superfrost Plus slides, dehydrated and coverslipped with Permount (Fischer Scientific, Electron Microscopy Sciences, Washington, PA, USA).

The specificity of the immunohistochemical labeling was tested for each primary antibody or antiserum: 1) by incubating some sections from control and pilocarpine-treated animals in a solution containing mouse or rabbit normal IgG (from Vector), instead of the primary antibody or antiserum, and 2) by incubating some sections in a solution omitting the primary antibody or antiserum. In all cases, no specific staining was detected under these conditions.

#### 2.3.2. Double immunofluorescence labeling for α-actn-2 and Prox-1

For double labeling, sections were processes as previously described (Soussi et al., 2015). Briefly, sections were incubated in a mixture containing α-actinin and Prox-1 antibodies and after several rinses in PB, they were incubated in a mixture of the following secondary antibodies: Alexa 488-conjugated goat anti-mouse IgG (1:200), and Cy3-conjugated goat anti-rabbit IgG (1:200) both from Jackson Immunoresearch (West Grove, PA, USA). All sections were mounted on superfrost slides, dried, and coverslipped with Fluoromount G (Southern Biotechnology Associates, Birmingham, AL, USA). Immunohistochemical controls for double-labeling experiments included incubation of some sections in a mixture of one primary antibody and normal IgG (mouse/rabbit normal IgG). In all cases, these sections exhibited the same pattern of immunolabeling as sections processed for single labeling. The specimens were then analyzed using a confocal microscope (Zeiss, LSM 700, Germany) and images were acquired using Zen software (Zeiss, Jena, Germany), and processed using Adobe Photoshop and *ImageJ* softwares.

### 2.4. In situ hybridization histochemistry

#### 2.4.1. Probe synthesis

The α-actn-2 probes used in this study were digoxigenin-labeled riboprobes obtained by *in vitro* transcription of a rat full-length actn-2 cDNA (NCBI accession number NM_001170325). The DNA templates for synthesizing RNA probes to α- actn-2 mRNA were constructed using RT-PCR (Reverse Transcriptase-Polymerase chain reaction (PCR) strategy, using a sense primer (position 190-213; 5'atgaatcagatagagcccggcgtg3') and an antisense primer (2848-2872; 5' gccctctacggggagagcggacctc 3'), as described previously (Sbai et al., 2012). This cDNA of 2682 bp was inserted into the pCR TOPO II vector (Invitrogen, Burlingame, CA, USA) and the construct was subsequently fully sequenced to verify the integrity of the α-actn-2 cDNA insert and to determine its orientation. The recombinant plasmid containing the α-actn-2 cDNA insert was linearized with the restriction enzyme BamHI and transcribed with T7 RNA polymerase to obtain the sense probe or linearized with EcoRV and transcribed with Sp6 to obtain the antisense probe. The transcription was carried out with the nonradioactive RNA labeling kit (Roche Diagnostics, Meylan, France), as previously described (Esclapez et al., 1993; Ferhat et al., 1998a, 1998b). Briefly, the sense and antisense transcripts labeled with digoxigenin-11-UTP were digested by alkaline hydrolysis for 30 min in order to obtain probes of approximately 150 nucleotides in length.

The labeling efficiency of the digoxigenin-labeled probes for both mRNAs was determined each time by direct immunological detection on dot blots with a nucleic acid detection kit (Roche Diagnostics). The intensity of the signal for each probe was compared with a serial dilution of digoxigenin-labeled control RNA of known concentration. Only sense and antisense α-actn-2 probes with comparable signal intensity (comparable labeling efficiency), as determined in dot blots, were used for *in situ* hybridization.

#### 2.4.2. Hybridization and detection

Free-floating sections were processed for α-actn-2 *in situ* hybridization according to a previously described protocol (Esclapez et al., 1993; Boulland et al., 2007). Sections were incubated overnight at 50°C in the hybridization solution containing 0.2 ng/μl of the digoxigenin labeled RNA probes (antisense or sense control). Low- to high-stringency washes were performed with decreasing concentrations of SSC, ending with an incubation in 0.1X SSC, 10 mM sodium thiosulfate for 30 min at 55°C. Sections were then processed for immunodetection of the digoxigenin label by means of a nucleic acid detection kit (Roche Diagnostics) and chromogen solution containing nitroblue tetrazolium (NBT) and 5-bromo-4-chloro-3-indolyl phosphate (BCIP) reagents. Incubation times in the chromogen solution were determined according to two different protocols (Esclapez and Houser, 1999). In one set of experiments, sections from control (Ctl) and pilocarpine-treated animals were incubated in the chromogen solution until optimal staining was achieved in each of the 4 animal groups (control, 1 week, 2 weeks, and chronic pilocarpine-treated rats). For the α-actn-2 probe, the optimal color-reaction times (24 h) were similar for all sections from all animal groups. A second set of experiments was performed to compare directly the differences in levels of labeling for mRNA-containing neurons between the four animal groups. Sections from these groups were incubated for identical times in the chromogen solution. Series of sections from all groups that were processed identically were removed from the chromogen solution at three time intervals for α-actn-2 probe (6, 12 and 24 h) to compare the labeling intensities among sections from the four animal groups at each interval. The differences in the levels of labeling in relation to the color-reaction times have been discussed previously and reflect differences in the amounts of mRNA (Esclapez et al., 1993; Ferhat et al., 1998b; Esclapez and Houser, 1999). In all experiments, the color reaction was stopped by rinsing the sections in 10 mM Tris HCl, pH 8.0, with 1 mM ethylene diamine tetraacetate (EDTA). Sections were then mounted on superfrost slides, dried, and coverslipped in an aqueous mounting medium (Crystal/Mount; Biomeda, Foster City, CA, USA).

### 2.5. Subcellular fractionation and Western Blot analysis

Ctl and pilocarpine-treated rats were rapidly decapitated and hippocampi were quickly dissected out from brains into ice-cold PB. For subcellular fractionation, both hippocampi of each Ctl (n=3) and pilocarpine-treated (n=3) rats were disaggregated into 10 volumes of cold homogenization buffer (320 mM sucrose, 10 mM Hepes, ph 7.4, 2 mM EDTA, protease inhibitors, 1/100, and 10 mM β-Glycerophosphate) using p1000 tips followed by p100 tips. Samples were sonicated using

two 5-second pulses. To remove pelleted nuclear fraction, samples were centrifuged at 1000 x g for 5 min at 4°C. All hippocampal supernatants were then centrifuged at 200000 x g for 30 min at 4°C to yield cytosolic fractions (C) and membrane fractions (M). The membrane fractions were re-suspended in 1/3-1/4 of the original volume of the homogenate. The cytosolic and membrane fractions were then separated into aliquots and protein concentrations were then determined by the DC protein assay (Biorad, Hercule, CA, USA) according to the manufacturer's protocol. After 5 min boiling, laemmli buffer with 6% 2-mercaptoethanol was added to aliquots containing equal amounts of protein which were resolved on 10% sodium dodecyl sulfate (SDS)-polyacrylamide gel electrophoresis (PAGE) using a MiniBlot system (Bio-Rad). After electrophoresis, the proteins were transferred onto Hybond-ECL nitrocellulose membranes (Amersham Biosciences, Buckinghamshire, UK) in transfer buffer (25 mM Tris, 192 mM glycine, 20% ethanol). Before blocking, the blots were stained with ponceau red to visualize transfer efficiency. The blots were then blocked in Tris-buffered saline (TBS and 0,05% tween 20, TBS-T) containing 5% milk for 1 h at RT and sequentially incubated overnight at 4°C in TBS-T containing 5% milk and following primary antibodies: mouse monoclonal α-actinin antibody (1/2000, sigma) or rabbit polyclonal antibody α-actinin (1/1000, abcam, Paris, France); rabbit polyclonal drebrin antibody (1/1000, sigma); mouse monoclonal GAPDH antibody (1/5000, millipore, Guyancourt, France); mouse monoclonal β-actin antibody (1/10000, Sigma); mouse monoclonal NTSR3 antibody (1/200, Santa cruz, Dallas TX, USA) and goat polyclonal NR1 antibody (1/400, Santa cruz). After incubation with primary antibodies, blots were washed three times for 5 min in TBS-T, incubated with corresponding horseradish peroxidase (HRP) secondary antibodies all from Jackson ImmunoReasearch: goat anti-mouse IgG-HRP (1/1000), goat anti-rabbit IgG Fc-HRP (1/10000); rabbit anti-goat IgG-HRP (1/2000) and rabbit anti-mouse IgG (1/2000) in TBS-T containing 5% milk for 1 h at RT and washed three times for 5 min each with TBS-T. Finally, proteins were detected using a chemiluminescence kit (ECL prime, Roche Diagnostics) and visualized using chemiluminescence imaging system (UVITEC CAMBRIDGE, England, UK). Chemiluminescent signals were then quantified using Image*J* software. Data are presented as a percentage of control values, considered as being 100% and are expressed as means ± S.E.M from at least three separate experiments.

### 2.6. Cell line, transfection and immunofluorescence

Chinese Ovary (CHO-K1) cells were obtained from the American Type Tissue Culture Collection (ATCC, Molsheim, France). They were grown in F12 (Invitrogen, Cergy Pontoise, France), supplemented with 10% Fetal Bovine Serum (FBS, Invitrogen), 2 mM glutamine (Invitrogen), 100 i.u./ml penicillin and 100 mg/ml streptomycin (Sigma) and were transiently transfected with either 1 μg of α-actn-2-RFP or 1 μg α-actn-2-RFP and 1 μg drebrin A-GFP (DA-GFP) constructs using Jet PEI (Polyplus) according to the manufacturer's protocol (Ozyme, Illkirch, France). Twenty-four hours after transfection, cells were fixed with 4% PFA in PB for 20 min at RT.

For the F-actin staining, the cells expressing α-actn-2-RFP were incubated with 0.5% Triton X-100 and 1% BR for 30 min and exposed for 2 h at RT to 0.5 unit per coverslip of Alexa-488 phalloidin (Molecular Probes, Leiden, Netherlands). Cells were rinsed in PB and then mounted with Fluoromount G.

Image acquisition was performed on a Zeiss laser-scanning microscope. Images of α-actn-2-RFP/F-actin or α-actn-2-RFP/DA-GFP were obtained using the 488 nm band of an Argon laser and the 594 nm bands of a solid state laser for excitation. Fluorescence images were acquired by sequential scanning using 63 X 1.32 oil immersion lens (zoom 1) and processed with Adobe Photoshop software.

### 2.7. Primary cultures of rat hippocampal neurons and transfection

The primary hippocampal cells (mixed culture) were prepared from embryonic day 18 (E18) rats and cultured in Neurobasal supplemented with 2% B-27, 1% penicillin-streptomycin, and 0.3% glutamine in a humidified atmosphere containing 5% CO2 at 37°C. At 21 days *in vitro* (div), when neurons displayed mature morphological and physiological features (Ivanov et al., 2009b), hippocampal cultures were transiently transfected with GFP or DA-GFP using lipofectamine 2000 reagent according to manufacture protocol (Invitrogen). Forty-eight hours following transfection, the cells were fixed with 4% PFA in PB for 20 min at RT and immunostained for endogeneous α-actn-2. Image acquisition was then performed using Zen software (Zeiss, Jena, Germany), and processed using Adobe Photoshop and *ImageJ* softwares.

### 2.8. Data analysis

All histo- and cytochemical quantifications were performed blindly. Qualitative and semi-quantitative analyses of the levels of immunolabeling for α-actn-2 were conducted in the outer molecular layer (OML), inner molecular layer (IML) of the dentate gyrus (DG), granule cell layer (G), and hilus (H) to identify differences between Ctl (n=6 rats) and pilocarpine animals (1w: n=6 rats; 2w: n=6 rats; 12 weeks: n=4 rats). This analysis of labeling intensity was performed by optical densitometric measurements of the labeling with an image analyzing system according to previously described methods (Esclapez and Houser, 1999; Ferhat et al., 2003; Sbai et al., 2012). The image analysis system used in this study included a PC-compatible computer, a Nikon digital camera DXM 1200 connected to an Eclipse E800 light microscope, a Nikon ACT-1 frame grabber, and *ImageJ* software. All images were acquired under the same conditions of light illumination, with a stabilized microscope light source, and at a final digitized size of 640 x 480 pixels. The densitometric analysis of labeling was performed using *ImageJ* software, which automatically determined the gray-level value. For each Ctl and pilocarpine animal, quantitative data were obtained from the dentate gyrus on both sides in 4 sections. For each dentate gyrus, the analysis of labeling intensity was performed from a total of 10 microscopic fields (minimum of 240) per region of interest. For each of these microscopic fields, the total gray-level value was automatically obtained. The gray-level value of the corpus callosum was used as a reference value for background. The specific intensity of labeling corresponding to the corrected gray-level value was calculated by subtracting the gray-level value of the background from the total gray-level value. The corrected gray-level values of Ctl and pilocarpine animals were then normalized on the mean value of Ctl animals. For each region of interest, the mean and corresponding standard error to the mean (S.E.M) intensity of labeling obtained from the total number of microscopic fields were calculated for each series of Ctl and pilocarpine-treated animals. A detailed qualitative and semi-quantitative analysis of the labeling intensity of α-actn-2 mRNA-containing neurons was performed on G and H as previously described for immunohistochemistry to identify differences between Ctl (n=6 rats) and pilocarpine animals (1w: n=4 rats; 2w: n=4 rats; 12 weeks: n=4 rats).

Ectopic hilar Prox-1-immuno-labeled cells were subjected to blind counting analysis on digitized images using *imageJ* software. The region of interest was selected manually using area selection tool. Counts were made from 3-4 rats/group using 3 sections (18-24 dentate gyri) spanning the entire hilus region. The mean number of hilar Prox-1-labeled cells in pilocarpine-treated animals was compared with mean value of saline-treated animals.

To quantify the data from the immunocytochemistry, regions of interest containing pyramidal-shape neurons were chosen randomly for image acquisitions from separate experiments. In order to compare the different experiments, all pictures were taken with the same parameters. Three to four transfected neurons were chosen randomly from 3 independent experiments for GFP and DA-GFP constructs and the total

fluorescence intensity of α-actn-2 was collected from their cell bodies and from at least three dendritic segments of 100 μm per neuron using *imageJ* software. The mean immunofluorescence intensity of α-actn-2 in the dendrites and the cell bodies of DA-GFP neurons were compared with the mean value of GFP control neurons represented as 100 AU.

### 2.9. Statistical analysis

Sample sizes and statistical power were determined according to Dell et al. (2002) and Festing and Altman (2002) using biostaTGV site (http://biostatgv.sentiweb.fr/?module=etudes/sujets#).

Student's *t*-test was used to compare two groups as previously described in Sharvit et al. (2013). ANOVA analysis followed by a Tukey's *post hoc* test was used for multiple comparisons. All data were expressed as the mean ± S.E.M. Statistical significance was set up to * $p<0.05$, ** $p<0.01$, and *** $p<0.001$.

## 3. Results

### 3.1. α-actn-2 protein is expressed in adult rat hippocampus

In the Ctl adult rats, α-actn-2 immunolabeling showed a regional- and laminar-specific pattern within the hippocampal formation (Fig. 1A), as previously described (Wyszynski et al., 1998; Dunah et al., 2000).

A detailed analysis in the hippocampus showed that while the α-actn-2 immunolabeling was moderate in the stratum oriens (O), stratum radiatum (R), the stratum lacunosum-moleculare (LM) of the CA1-CA3 areas and in the hilus (H), the molecular layer (ML) of the dentate gyrus (DG) and the dendritic layers of CA2 displayed stronger α-actn-2 immunolabeling (Fig. 1A). Similarly, the cell bodies of hippocampal pyramidal neurons were weakly labeled in CA1 and CA3, whereas they were strongly immunolabeled in CA2 (Fig. 1A, see arrowheads in inset). The α-actn-2 immunohistochemical labeling was abolished when the EA-53 α-actn-2 antibody was omitted (data not shown). Scattered cell bodies highly immunolabeled for α-actn-2 were also observed in the stratum lacunosum-moleculare of CA1 (Fig. 1B, see arrowheads in b1 inset). In the dentate gyrus, at lower magnification, α-actn-2 labeling was homogeneous in the molecular layer (M) and hilus (Fig. 1A). Some processes immunolabeled for α-actn-2 likely corresponding to granule cell dendrites were observed in the inner molecular layer (IML) (Fig. 1B, see black arrowheads). At higher magnification, this labeling appears punctiform (Fig. 1B, see white arrowheads in b3 and b4 insets). In the granule cell layer (G), most of the cell bodies were weakly labeled but several scattered cells located within this layer, along the infragranular border of the dentate gyrus as well as in the hilus were strongly labeled for α-actn-2 (Fig. 1B, see arrows in b2 inset). Part of these scattered cells located in the dentate gyrus and hilus could correspond to interneurons as previously reported (Wyszynski et al., 1998; Ratzliff and Soltesz, 2001).

### 3.2. Hippocampal α-actn-2 protein expression is altered in the pilocarpine-treated rats

The α-actn-2 labeling pattern was altered in pilocarpine animals (Fig. 2C-H) at all time points analyzed compared to that observed in Ctl rats (Fig. 2A, B). The main difference between Ctl animals (Fig. 2A, B) and pilocarpine rats at 1 week (Fig. 2C, D) and 2 weeks (Fig. 2E, F) was observed in the inner molecular layer, as well as in the granule cell layer and hilus of the dentate gyrus. Indeed, quantitative analysis showed that in the inner molecular layer, the mean intensities of α-actn-2 labeling were reduced in the pilocarpine rats at 1 week (80.26 ± 1.49%, 19.74%; $P < 0.01$; Tukey's test), 2 weeks (77.36 ± 1.16%, 22.64%; $P < 0.01$; Tukey's test) and 12 weeks (81.48 ± 1.24%, 18.52; $P < 0.01$; Tukey's test) when compared with Ctl rats (100 ± 1.51%) (Fig. 2I). The loss of labeling in the inner molecular layer contrasted with the preserved

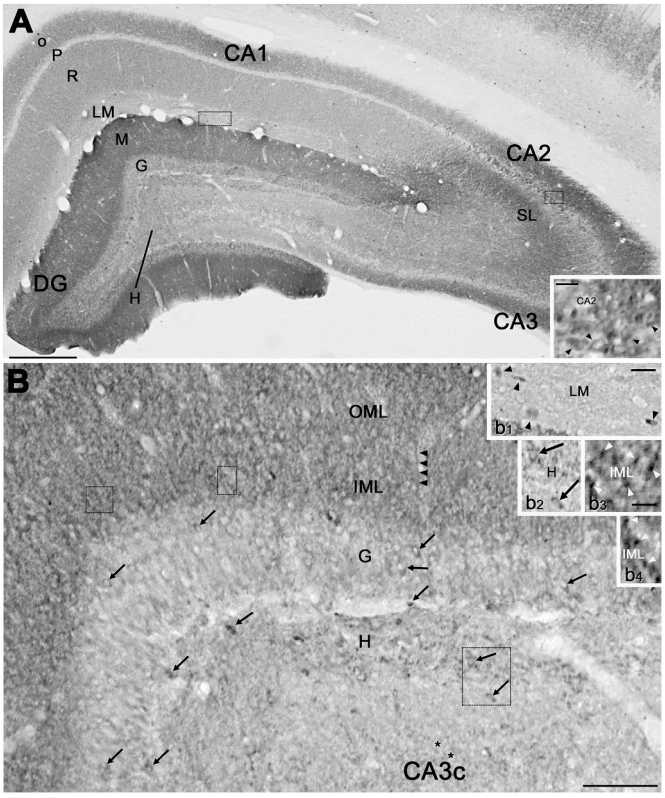


**Fig. 1.** immunohistochemical labeling of adult rat hippocampus. A: Coronal section of the rat brain processed with α-actn-2 antibody EA-53 and revealed by immunoperoxydase labeling. Low magnification pictures showing regional and laminar differences in immunoreactivity in the hippocampus (A). While the α-actn-2 immunolabeling was moderate in the stratum oriens (O), stratum radiatum (R), the stratum lacunosum-moleculare (LM) of the CA1-CA3 areas and in the hilus (H), the molecular layer (ML) of the dentate gyrus (DG) and the dendritic layers of CA2 displayed stronger α-actn-2 immunolabeling (A). The cell bodies of hippocampal pyramidal neurons were weakly labeled in CA1 and CA3 (A), whereas they were strongly immunolabeled in CA2 (A, see arrowheads). Scattered interneurons were intensely immunolabeled for α-actn-2 in the stratum lacunosum-moleculare of CA1 (B, see black arrowheads in b1) as well as in the hilus (B, see arrows in b2). Note that few cells located within granule cell layer (G) and along the infragranular border of the dentate gyrus were also labeled for α-actn-2 (B, see arrows). In addition, high magnification pictures (B) show that α-actn-2 immunolabeling appears punctiform in the molecular layer (M) (B, see white arrowheads in IML in b3 and b4 insets). Scale bars : 500 μm in (A); 30 μm in inset in A, 100 μm in (B) and 30 μm in b1 and b2 insets, 10 μm in b3 and b4 insets.

levels of labeling we observed in two-thirds of the outer molecular layer (OML) (100 ± 1,42% in Ctl, 94,73 ± 1,66% at 1 week, 96,75 ± 1,21% at 2 weeks and 102,78 ± 1,40% at 12 weeks; $P > 0.05$; ANOVA) (Fig. 2I). In the granule cell layer, the mean intensities of α-actn-2 immunolabeling were increased in the pilocarpine animals at 2 weeks (106.66 ± 1.36%, 7%; $P < 0.05$; Tukey's test) when compared with Ctl rats (100 ± 1.76%), while no difference was observed in pilocarpine-treated animals at 1 week (97.35 ± 1.68%, $P > 0.05$; ANOVA) and 12 weeks (99.34 ± 1.61%, $P > 0.05$; ANOVA) (Fig. 2I). Similar to our observations in the inner molecular layer, the mean intensities of labeling in the hilus were decreased in pilocarpine animals at 1 week (88.06 ± 1.67%, 11.94%; $P < 0.01$; Tukey's test) and at 2 weeks (85.42 ± 1.68%, 14.58%; $P < 0.01$; Tukey's test), when compared to Ctl rats (100 ± 1.71%), whereas an increase was observed in pilocarpine rats at 12 weeks (107,25 ± 1.64%; 7%; $P < 0.05$; Tukey's test) (Fig. 2I).

All together our data suggested that decreased α-actn-2 labeling in the inner molecular layer was associated with neo-spinogenesis and morphogenesis previously described in the pilocarpine model used in

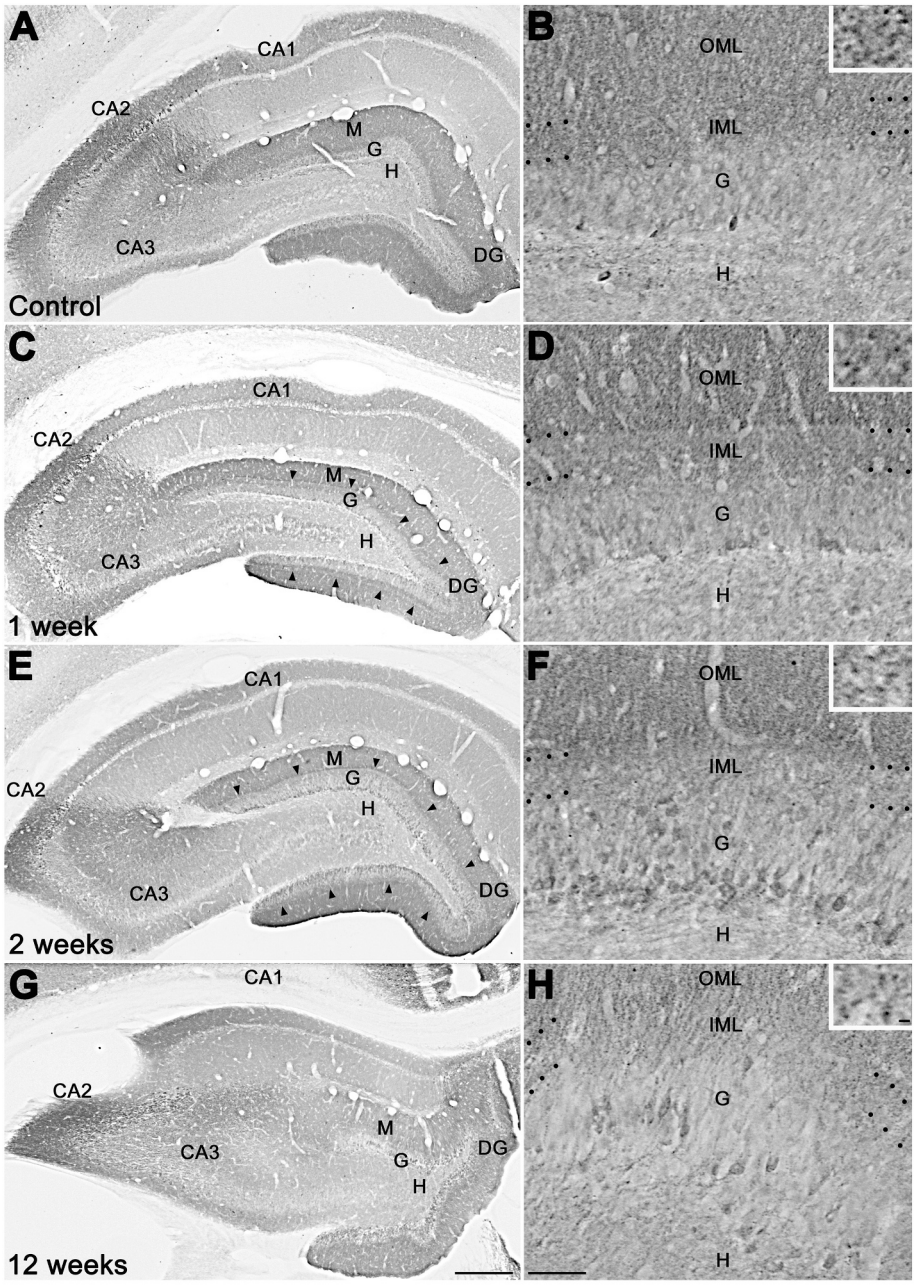


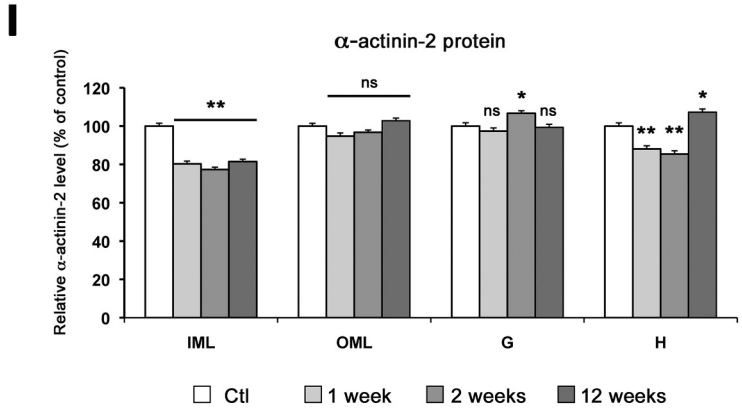


**Fig. 2.** Comparison of immunolabeling for α-actn-2 in coronal sections of the hippocampal formation from control (Ctl; n= 6 rats; A and B) and pilocarpine animals at 1 week (n= 6 rats; C and D), 2 weeks (n= 6 rats; E and F), and 12 weeks (n= 4 rats; G and H). The profile of immunolabeling for α-actn-2 was clearly modified in pilocarpine animals (D, F and H) at all time points compared to Ctl rats (B). The main difference between pilocarpine animals and Ctl animals (A and B) was observed in the molecular layer (M), the granule cell layer (G) and the hilus (H) of the dentate gyrus (DG). Insets in B, D, F, and H correspond to high magnification of the inner molecular layer (IML) of the dentate gyrus. The labeling for α-actn-2 appears punctiform (see insets). Scale bars : 450 μm in (A, C, E, and G); 90 μm in (B, D, F, and H); 10 μm in insets. I) Histograms comparing the mean intensities of immunolabeling for α-actn-2 in the inner molecular layer (IML), outer molecular layer (OML), granule cell layer (G), and hilus (H) of the dentate gyrus (DG) from Ctl and pilocarpine-treated animals at 1 week, 2 weeks, and 12 weeks. Statistically significant differences in the mean estimated intensity of labeling are indicated (*$P < 0.01$, **$P < 0.001$; ANOVA with a post hoc Tukey's test). All data were expressed as the mean ± S.E.M.

our study (Isokawa and Mello, 1991; Isokawa, 1998, 2000; Kurz et al., 2008), whereas the reduced α-actn-2 labeling observed in the hilus could be associated with the loss of some subpopulations of hilar neurons occurring during epileptogenesis (Sloviter, 1987; Obenaus et al., 1993; Buckmaster et al., 2002; Boulland et al., 2007; Houser, 2014).

Many studies have reported that dentate granule cells are relatively well preserved in the pilocarpine model we used (Mello et al., 1993; Obenaus et al., 1993; Debski et al., 2016). Thus using *in situ*

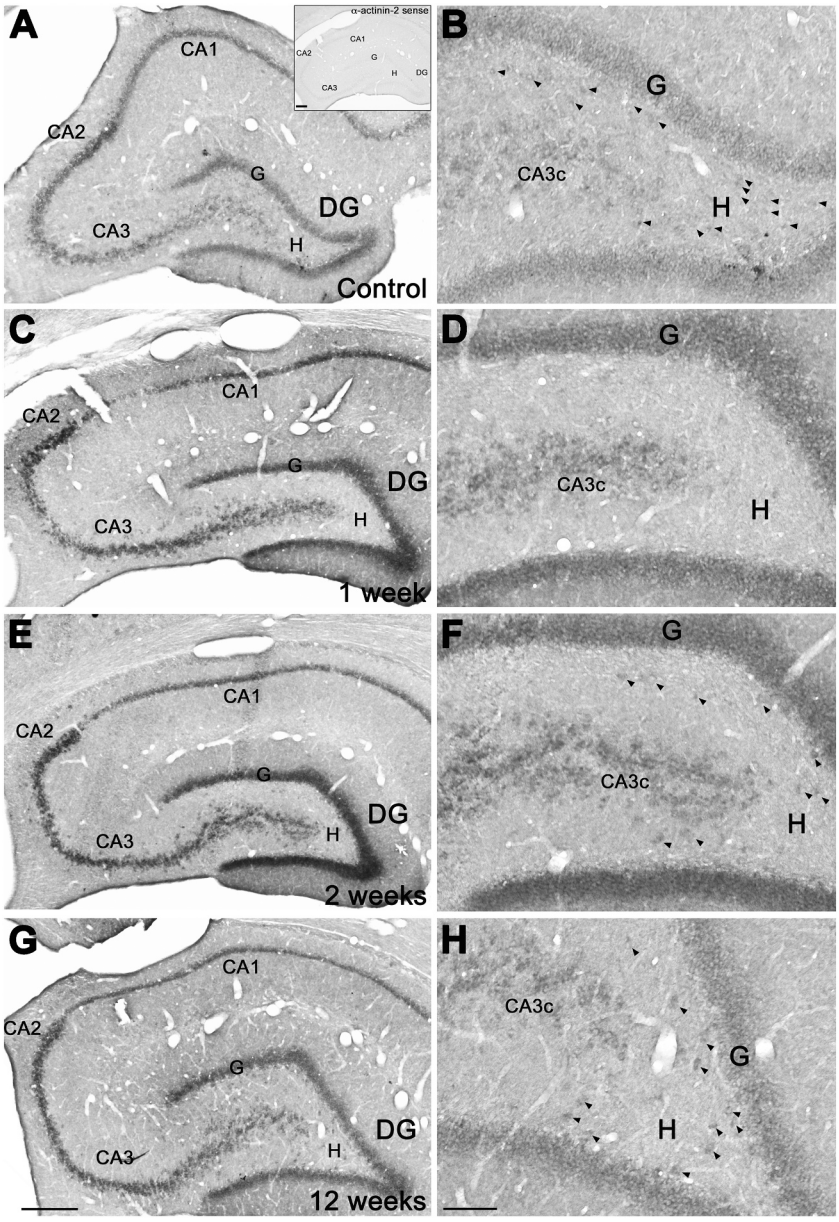


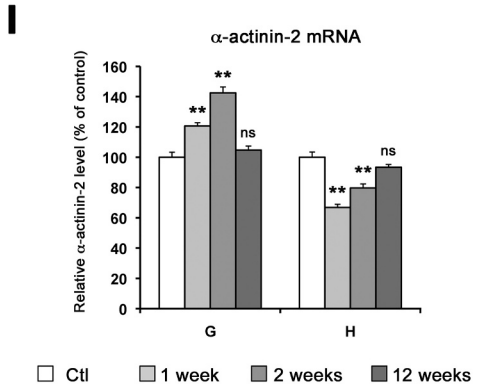


**Fig. 3.** Comparison of α-actn-2 mRNA expression in coronal sections of the hippocampal formation from control (Ctl; n= 6 rats; A and B) and pilocarpine rats at 1 week (n= 6 rats; C and D), 2 weeks (n= 6 rats; E and F), and 12 weeks (n= 4 rats; G and H) processed for the same color reaction time. (A-H) correspond to sections processed with antisense RNA probe. Inset in A corresponds to a section processed with the sense Ctl RNA probe. No staining is observed with the sense probe in the hippocampal formation. In all pilocarpine animals (C-H), the main difference compared to Ctl animals (A and B) is observed in the hilus (H) and in the granule cells of the dentate gyrus (DG). Scale bars : 450 μm in (A, C, E and G); 90 μm in (B, D, F and H); 100 μm in inset in A. I : Histogram comparing the mean intensities of α-actn-2 mRNA in the hilus and granule cell layer of the dentate gyrus from Ctl and pilocarpine animals at 1-, 2-, and 12 weeks. Statistically significant differences in the mean estimated intensity of labeling are indicated (*$P < 0.05$, **$P < 0.01$; ANOVA with a post hoc Tukey's test). All data were expressed as the mean ± S.E.M.

hybridization for α-actn-2 mRNA, we further investigated whether α-actn-2 protein decrease observed in the IML of the pilocarpine rats reflected granule cell dendritic spine plasticity rather than loss of dentate granule cells.

### 3.3. Hippocampal α-actn-2 mRNA expression is altered in the pilocarpine-treated rats

The levels of α-actn-2 mRNA labeling within the hippocampal formation were compared between pilocarpine and Ctl rats. *In situ* hybridization analysis using a digoxygenin-labeled antisense probe for α-actn-2 showed moderate to strong labeling of the α-actn-2 mRNA containing cells in the hippocampus of Ctl animals. This α-actn-2 labeling was restricted to CA1, CA2, and CA3 pyramidal cell layers (Fig. 3A) and the granule cell layer of the dentate gyrus (Fig. 3A, B), as previously reported (Dunah et al., 2000). In addition to the principal cells, several hilar cells of the dentate gyrus were also labeled for α-actn-2 mRNA (Fig. 3B, see arrowheads) that could correspond to interneurons (Freund and Buzsáki, 1996; Houser, 2007) and/or mossy cells (Amaral, 1978). No labeling was detected with the digoxygenin-labeled sense control probe (Fig. 3A, see inset).

In all pilocarpine rats, the labeling patterns for α-actn-2 mRNA were altered compared to Ctl rats (Fig. 3) at all color reaction times examined. These differences in labeling intensity of α-actn-2 mRNA between pilocarpine-treated and Ctl animals were consistently observed in all animals and regions examined including the granule cell layer and hilus of the dentate gyrus. Quantitative data showed that, in granule cell layer, the mean intensities of α-actn-2 mRNA labeling were increased in the pilocarpine animals at 1 week (120.58 ± 2.16%, 20.6%; $P < 0.01$; Tukey's test) and 2 weeks (142.50 ± 3.9%, 42.50%; $P < 0.01$; Tukey's test), when compared to Ctl rats (100 ± 3.30%) (Fig. 1I). However, no difference in α-actn-2 mRNA was observed in the granule cell layer between Ctl rats and 12 weeks pilocarpine-treated animals (104,70 ± 2.64, 4.70%; $P > 0.05$; ANOVA; Fig. 3I). In contrast to the granule cell layer, the mean intensities of α-actn-2 mRNA labeling were decreased in the hilus of the pilocarpine animals at 1 week (66.86 ± 2.06%, 44.76%, $P < 0.01$; Tukey's test) and 2 weeks (79.70 ± 2.66, 40.19%; $P < 0.01$; Tukey's test), when compared with Ctl rats (100 ± 3.45%) (Fig. 3I). No difference was observed between Ctl and 12 weeks pilocarpine rats (93.37 ± 1.83%, 6,63%; $P > 0.05$; ANOVA) (Fig. 3I). In addition, the increased expression levels of α-actn-2 mRNA in the granule cell layer observed 1-2 weeks (Fig. 3I) after injection of pilocarpine translated into a significant increase of α-actn-2 immunolabeling in the granule cell layer and hilus only in pilocarpine animals at 2- and 12 weeks respectively (Fig. 2I). Interestingly, several cells located at the base of granule cell layer and/or in the hilus, which were only weakly labeled in Ctl animals, showed clearly increased levels of α-actn-2 mRNA in pilocarpine animals at 2 weeks (compare A and B with E and F, see arrowheads) and 12 weeks (compare A and B with G and H, see arrowheads).

The increased levels of α-actn-2 mRNA within the granule cell layer further suggested that the α-actn-2 protein decrease in the inner molecular layer was associated with dendritic spine plasticity of granule cells rather than with a loss of dentate granule cells.

In the course of epileptogenesis, the temporal profile of α-actn-2 immunolabeling shows a significant decrease in the inner molecular layer at the latent period, which did not return to Ctl levels at the chronic stage. We hypothesize that α-actn-2 is not critical for stabilization and structural integrity of mature dendritic spines observed at this chronic stage, in contrast with DA, another actin-binding protein (Ferhat, 2012; Sbai et al., 2012), known to reorganize and stabilize F-actin (Ivanov et al., 2009a, 2009b; Mikati et al., 2013; Worth et al., 2013). To test this hypothesis, we analyzed the effects of α-actn-2 on the organization and stabilization of F-actin in CHO-K1 cells and its interaction with DA in CHO-K1 cells and in neurons transfected with GFP, DA-GFP and/or α-actn-2-RFP.

### 3.4. α-actn-2-RFP did not reorganize F-actin

F-actin organization was examined in CHO transfected cells using Alexa Fluor 594/488 phalloidin. Control GFP transfected cells (Fig. 4A1) showed actin stress fibers (see arrowheads) crossing over the cytoplasm, and bundles of F-actin (see arrows) beneath the plasma membrane (Fig. 4A2). In addition, these GFP cells did not display any morphological alterations compared with DA-GFP transfected cells (Fig. 4B1). As we previously reported, overexpression of DA-GFP in CHO-K1 cells does not only alter the organization of the microfilaments, but also affects the general cell morphology (Ivanov et al., 2009a, 2009b; Ferhat, 2012). These DA-GFP cells displayed several cell processes often branched (Fig. 4B1, B2, see arrowheads). DA-GFP (Fig. 4B1) mainly co-localized with F-actin (Fig. 4B2, see insets in B1 and B2, yellow). In contrast to control GFP cells (Fig. 4A1), DA-GFP cells lost actin stress fibers (Fig. 4B2). Instead, thick and twisted bundles of F-actin were observed in the cytoplasm and/or within the cell processes (Fig. 4B1, B2, see arrowheads and insets in B1 and B2). In contrast to DA-GFP, the organization of the F-actin and the general cell morphology were not altered in α-actn-2-RFP cells. Indeed, α-actn-2-RFP cells (Fig. 4C1) displayed actin stress fibers within the cytoplasm (see arrows) and bundles of F-actin (see arrowheads) beneath the plasma membrane, similar to those observed in control GFP cells (Fig. 4A2). α-actn-2-RFP (Fig. 4C1) mainly co-localized with F-actin (Fig. 4C2, see arrows and arrowheads in C1 and C2 insets, yellow).

All together, these results indicated that α-actn-2-RFP did not alter the microfilament organization nor the general shape of the cells.

### 3.5. α-actn-2-RFP did not stabilize F-actin

To examine the stabilizing effects of α-actn-2-RFP on F-actin, GFP (Fig. 4A3), DA-GFP (Fig. 4B3) and α-actn-2-RFP (Fig. 4C3) expressing cells were treated with cytochalasin B, a microfilament-depolymerizing drug (Yahara et al., 1982; Cooper, 1987) for 15 min and F-actin was stained using Alexa Fluor 594/488 phalloidin (Fig. 4A4, B4, C4). In all un-transfected and GFP-transfected cells (Fig. 4A3), cytochalasin B treatment induced the fragmentation of cortical actin bundles and actin stress fibers (Edson et al., 1993; Ballestrem et al., 1998; Rami et al., 2006; Ivanov et al., 2009a, 2009b), since Alexa Fluor 594 phalloidin showed a patchy punctuate-like aggregation in the cytoplasm (Fig. 4A4, see arrowheads) and beneath the plasma membrane (Fig. 4A4, see arrows). However, in all DA-GFP cells (Fig. 4B3), the F-actin bundles in the cell body as well as within the processes were resistant to cytochalasin B treatment (Fig. 4B4) as underlined by the superimposition of DAGFP and F-actin (Fig. 4, compare panels B3 and B4). In contrast to DA-GFP (Fig. 4B3), CHO cells overexpressing α-actn-2-RFP treated with cytochalasin B displayed an altered F-actin network, similar to that observed in cytochalasin B treated GFP cells (Fig. 4A3). Indeed, α-actn-2-RFP (Fig. 4C3, see arrows in inset) still binds F-actin aggregates (short F-actin, Fig. 4C4, see inset, yellow) but does not protect actin filaments against cytochalasin B destabilization.

### 3.6. DA-GFP inhibits the binding of α-actn-2 on F-actin

We examined in non-neuronal and neuronal cell cultures whether DA competes with α-actn-2 for F-actin binding as shown by biochemical studies (test tube) (Ishikawa et al., 1994). To this end, DA-GFP (Fig. 4D1) and α-actn-2-RFP (Fig. 4D2) were first co-transfected in CHO-K1 cells and their distribution with respect to each other was analyzed. Our data showed clearly that α-actn-2-RFP did not bind to F-actin bundles induced by DA-GFP in the cytoplasm and/or within the cell processes (Fig. 4D3, see arrowheads in D3 inset), since the two proteins did not co-localize (see stars in Fig. 4D1, D2, D3). Instead α-actn-2-RFP aggregated in the cytoplasm (Fig. 4D2, see arrows in inset). Thus, our data indicated that DA competitively inhibits the actin-binding activity of α-actn-2 in CHO-K1 cells.

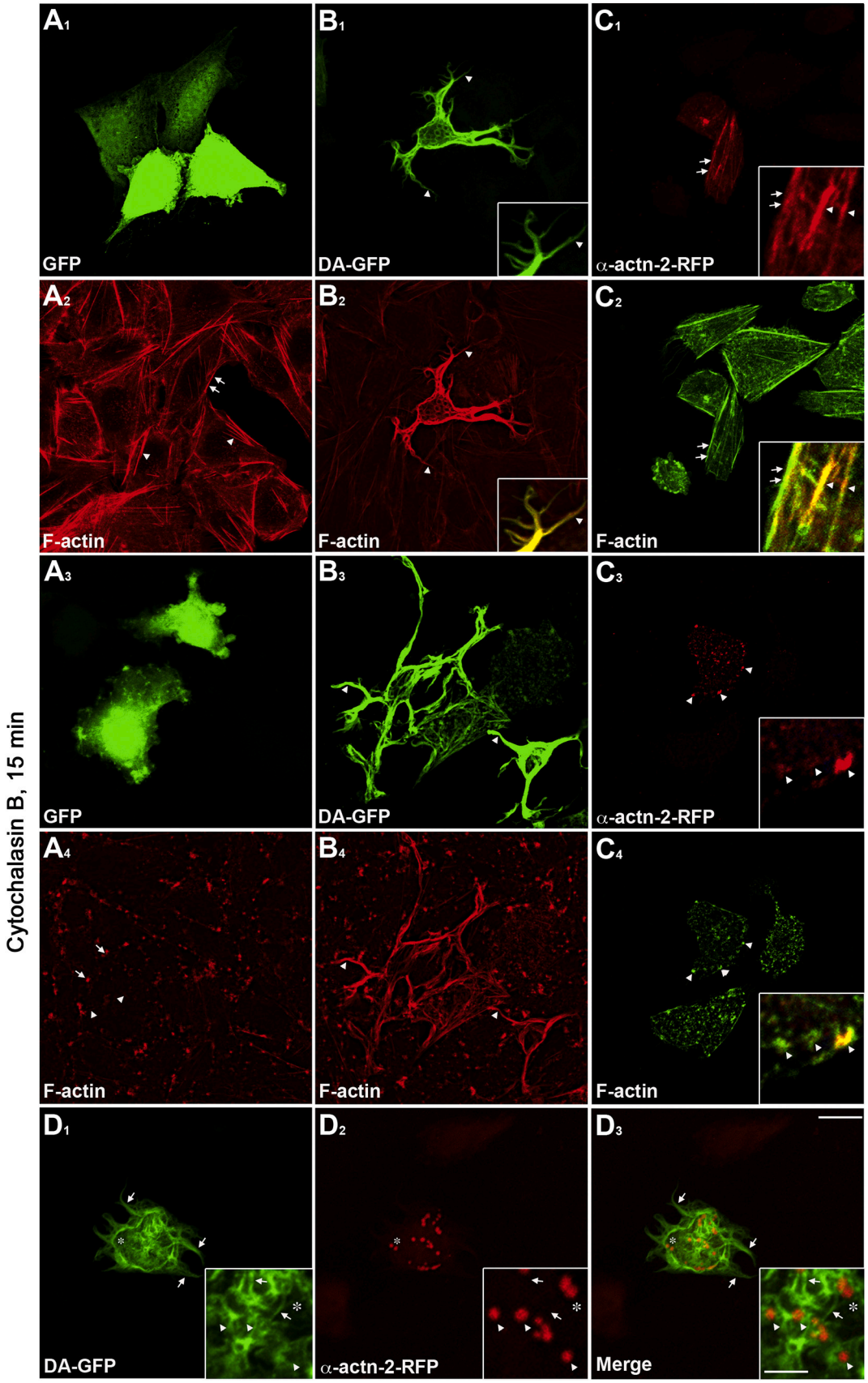


*(caption on next page)*

**Fig. 4.** Overexpression of drebrin A-GFP (DA-GFP) dissociates α-actinin-2-RFP (α-actn-2-RFP) from F-actin in CHO cells. CHO cells transfected with GFP (A1, green), DA-GFP (B1, green) and α-actn-2-RFP (C1, red) were stained with Alexa-488/594 phalloidin to assess F-actin organization (A2, red; B2, red; C2, green). Inset in panel C1 corresponds to high magnification of a cell process from a CHO cell expressing α-actn-2-RFP. Inset in C2 corresponds to the merge of α-actn-2-RFP and F-actin. α-actn-2-RFP (red) did co-localize with F-actin (green) (yellow, see arrows and arrowheads). Effects of the microfilament-depolymerizing drug cytochalasin B (10 μg/ml, 15 min) in cells transfected with GFP ($A_3$, green), DA-GFP ($B_3$, green), and α-actn-2-RFP ($C_3$, red). F-actin organization in these cells was assessed with Alexa-488/594 phalloidin ($A_4$, red; $B_4$, red; $C_4$, green). Inset in panel C3 corresponds to a region of the cell overexpressing α-actn-2-RFP and treated with cytochalasin B at high magnification. Inset in panel C4 corresponds to a region of the same cell overexpressing α-actn-2-RFP, treated with cytochalasin B, and labeled for F-actin. In cells treated with cytochalasin B, α-actn-2-RFP (red) co-localized with F-actin (green) (yellow, see arrowheads in inset of C4). CHO cell transfected with DA-GFP (D1, green) and α-actn-2-RFP (D2, red) shows that DA-GFP inhibits α-actn-2-RFP to bind to F-actin since the two proteins did not co-localize. Instead, α-actn-2-RFP aggregates (see arrowheads) into the cytoplasm. Inset in D1 corresponds to region of the cell overexpressing DA-GFP (green) at high magnification. Inset in D2 corresponds to the same region of the cell shown in inset of D1 overexpressing α-actn-2-RFP (D2, red) at high magnification. Inset in panel D3 corresponds to the merge of insets of D1 and D2. Scale bars : 10 μm in all panels and 3 μm in all insets.

We next examined whether DA could also inhibit the binding of α-actn-2 to F-actin in mature hippocampal neuron cultures. To this end, we overexpressed GFP (Fig. 5A) used as a control or DA-GFP (Fig. 5C) in mature cultured hippocampal neurons and analyzed the expression and distribution of endogenous α-actn-2 by confocal microscopy.

Confocal analysis revealed that both green fluorescent protein (GFP, used as a control) (Fig. 5A) and DA-GFP (Fig. 5C) were distributed within dendritic shafts as well as in dendritic protrusions. GFP fluorescence was equally homogenous between dendritic shafts and dendritic protrusions. In contrast, DA-GFP fluorescence in dendritic protrusions was higher than in dendritic shafts and dendritic necks. Remarkable morphological changes were also found in dendritic protrusions of DA-GFP- (Fig. 5C) when compared to those of GFP neurons (Fig. 5A). As a matter of fact, the dendrites of DA-GFP neurons exhibited longer protrusions (Fig. 5C, see c1 inset) as compared with the ones found in GFP neurons (Fig. 5A, see a1 inset). All protrusions induced by DA-GFP displayed heads suggesting that these long protrusions were dendritic spines. This pattern of expression of DA-GFP and related morphological changes were similar to those we previously described (Ivanov et al., 2009b; Ferhat, 2012).

The pattern of immunolabeling for α-actn-2 in GFP neurons was similar to that previously reported (Wyszynski et al., 1997, 1998; Biou et al., 2008; Hodges et al., 2014). As illustrated in Figure 5B, α-actn-2 immunolabeling was mainly punctiform in GFP neurons. Briefly, in GFP neurons (Fig. 5A, inset a1), α-actn-2 protein (Fig. 5B, inset b1) was localized in the cell bodies and particularly enriched within dendritic spines (Fig. 5B, see arrowheads in b2, yellow). However, in DA-GFP neurons (Fig. 5C), the pattern of α-actn-2 immunolabeling was clearly altered (Fig. 5D) compared to that in GFP neurons (Fig. 5B). Indeed, in DA-GFP neurons (Fig. 5C, inset c1), α-actn-2 protein (Fig. 5D, inset d1) was hardly seen in dendritic spines (Fig. 5D, see arrowheads in d2, green). Note also that only few α-actn-2 protein puncta (see arrows in Fig. 5D, inset d3, red) were observed within the cell bodies (highlighted with DAPI, blue, see insets d4 and d5 in Fig. 5D) of DA-GFP neurons (Fig. 5C, green). Quantitative analysis showed a decrease of the total fluorescence intensity for α-actn-2 in the dendrites (dendritic shafts and spines) (Fig. 5E, GFP: 100 ± 12.18%; DA-GFP: 41.30 ± 5.90%; 58.7%; $P < 0.001$; Student's *t test*) and in the cell bodies of DA-GFP neurons (Fig. 5F, GFP: 100 ± 17.35%; DA-GFP: 24.24% ± 7.15%; 75.76%; $P < 0.001$; Student's *t*-test) compared to those of GFP control neurons. Such results suggest that DA-GFP overexpression causes the release of α-actn-2 from F-actin that could lead to its degradation by proteases in hippocampal neurons, similar to what was observed in CHO-K1 cells. In all, our *in vitro* CHO and neuron experiments put forward cellular and molecular mechanisms that could be involved *in vivo,* in our pilocarpine model.

Furthermore, decrease of α-actn-2 expression could affect the membrane anchoring of NR1, known to interact with α-actn-2 (Wyszynski et al., 1997). To test this hypothesis, we used fractionation and Western blot techniques to investigate the co-regulation of NR1 and α-actn-2 expression levels in pilocarpine-treated rats at chronic stage, when DA, but not α-actn-2 (present results), had returned to control levels (Ferhat, 2012; Sbai et al., 2012).

### 3.7. α-actn-2 and NR1 levels are co-regulated in pilocarpine-treated rats

Before studying α-actn-2 and NR1 expression, we first validated our fractionation technique in our experimental conditions. Briefly, freshly isolated hippocampi from adult Ctl rats (n= 4 rats) were fractionated into cytosolic (C) and membrane (M) fractions. The purity of the fractions was assessed by Western blotting against specific markers: β-actin and GAPDH were used as major cytosolic markers (Baghirova et al., 2015). NTSR3 (neurotensin receptor 3/sortilin) (Béraud-Dufour et al., 2009; Mazella et al., 2010) and NR1 (Wyszynski et al., 1997, 1998; Reyes-Montaño et al., 2006; Henson et al., 2012) were used as membrane markers. Consistent with previous studies, NTSR3, NR1, β-actin, GAPDH, α-actn-2 (Wyszynski et al., 1997; Hodges et al., 2014), and DA (Sbai et al., 2012) proteins were detected as a single band with molecular weight of 100, 130, 42, 38, 100, and 120 kDa respectively, in Ctl and pilocarpine rats (Fig. 6A, B). We did not observe these bands when omitting the primary antibodies (data not shown). Our data showed that both β-actin and GAPDH are mainly present in the cytosolic fraction and at much lower levels in the membrane fraction (Fig. 6A). Both NTSR3 and NR1 were present in the membrane fraction of hippocampal tissue, but absent from the cytosolic fraction (Fig. 6A), confirming the membrane fraction enrichment.

In order to study the α-actn-2 and NR1 expression, we performed Western blotting analysis to follow the expression of α-actn-2, NR1, and DA in the hippocampal membrane fractions of Ctl (n=3) and 12 week pilocarpine-treated (n=3) rats (Fig. 6B). The same amounts (50 μg) of hippocampal membrane fraction from Ctl and 12 weeks pilocarpine rats were compared. NTSR3 was used as a control for normalization of protein loading because it has been shown to be enriched in membrane fraction (see Figure 6, panel A) and whose expression is not reduced at chronic stage (see Figure 6, panel B). Quantitative analyses showed that α-actn-2 and NR1 immunoreactivities were both decreased in the pilocarpine animals compared with Ctl rats (α-actn-2: 100% in Ctl, 34.9 ± 10.4% at 12 weeks; 65.1%; NR1: 100% in Ctl, 12.4 ± 3,7% at 12 weeks; 87.6%; $P < 0.001$; Student's *t*-test) (Fig. 6C, D). In contrast to α-actn-2 and NR1, DA immunoreactivy showed a tendency for decrease but differences did not reach statistical significance (100% in Ctl, 55.5 ± 29.6% at 12 weeks; $P > 0.05$; ANOVA) (Fig. 6E). These biochemistry data confirm our previous studies (Ferhat, 2012; Sbai et al., 2012). Indeed, these data showed that DA is significantly decreased at latent stage but returns to Ctl levels at chronic stage in all analyzed areas of the hippocampus using immunohistochemistry approaches. Thus, the Western blot data showed that in contrast to DA and NTSR3, α-actn-2 and NR1 levels are co-regulated in the membrane fraction of the chronic pilocarpine-treated rats.

Taken together, these data suggest that α-actn-2 contributes in the membrane anchoring of NR1.

### 3.8. The increased immunolabeling for α-actn-2 in the hilus at chronic stage occurred in the hilar ectopic dentate granule cells

In addition to the loss of α-actn-2 labeling in the inner molecular layer, we showed a significant increased immunolabeling for α-actn-2 in

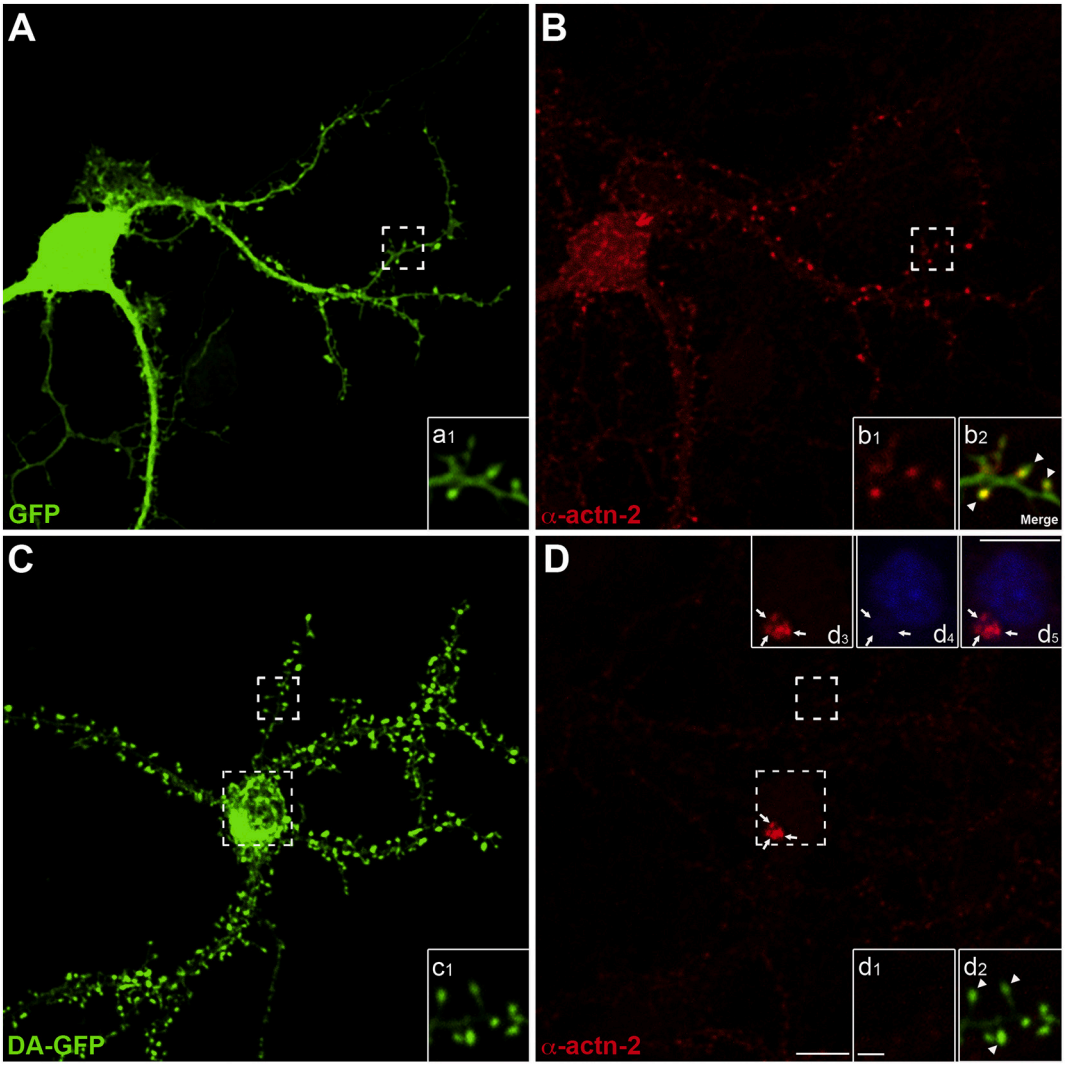



**Fig. 5.** Effects of DA-GFP overexpression on endogenous α-actn-2 expression and localization in mixed cultured of mature hippocampal neurons. Neurons were transfected at 21 div with control GFP (A and a1, green) or DA-GFP (C and c1, green) for 48 h. At 23 div, neurons were fixed and then immunostained for α-actn-2 (B, b1, D, d1 and d3, red). Insets a1 and c1 show higher magnification views of representative GFP and DA-GFP dendritic segments shown in A and C respectively. Insets b1 and d1 show the same region of the dendritic segment stained for α-actn-2 at high magnification. Insets b2 and d2 correspond to the merge of a1 and b1 color insets and c1 and d1 color insets respectively. Insets d3, d4, and d5 show higher magnification views of the same region of the cell body stained for α-actn-2 or DAPI or α-actn-2 and DAPI. *DAPI* was used for identifying DA-GFP cell bodies (see inset d4, blue). Inset d5 corresponds to the merge of insets d3 and d4. In GFP neurons (A and a1), α-actn-2 protein is mainly punctiform (B and b1). In GFP neurons (A and a1), α-actn-2 (B and b1) is localized in the cell body and mainly enriched within the dendritic spines (see arrowheads in b2, yellow) while in DA-GFP neurons (C and c1), α-actn-2 protein is hardly seen in dendritic spines (see arrowheads in d2, green), suggesting that DA-GFP overexpression prevents enrichment of α-actn-2 in dendritic spines. Note that some α-actn-2 protein puncta were found (see arrows in D, d3 and d5, red) within the cell body of DA-GFP neurons. The total fluorescence intensity of α-actn-2 in the dendritic shafts and spines (E) and in the cell bodies (F) was quantified. The average fluorescence intensity of α-actn-2 in the dendrites and the cell bodies of DA-GFP neurons were significantly lower than that of GFP control neurons. AU : Arbitrary unit. Scale bars : 10 μm in (A, B, C, D, d3, d4 and d5); 2 μm in (b1, b2, d1 and d2).

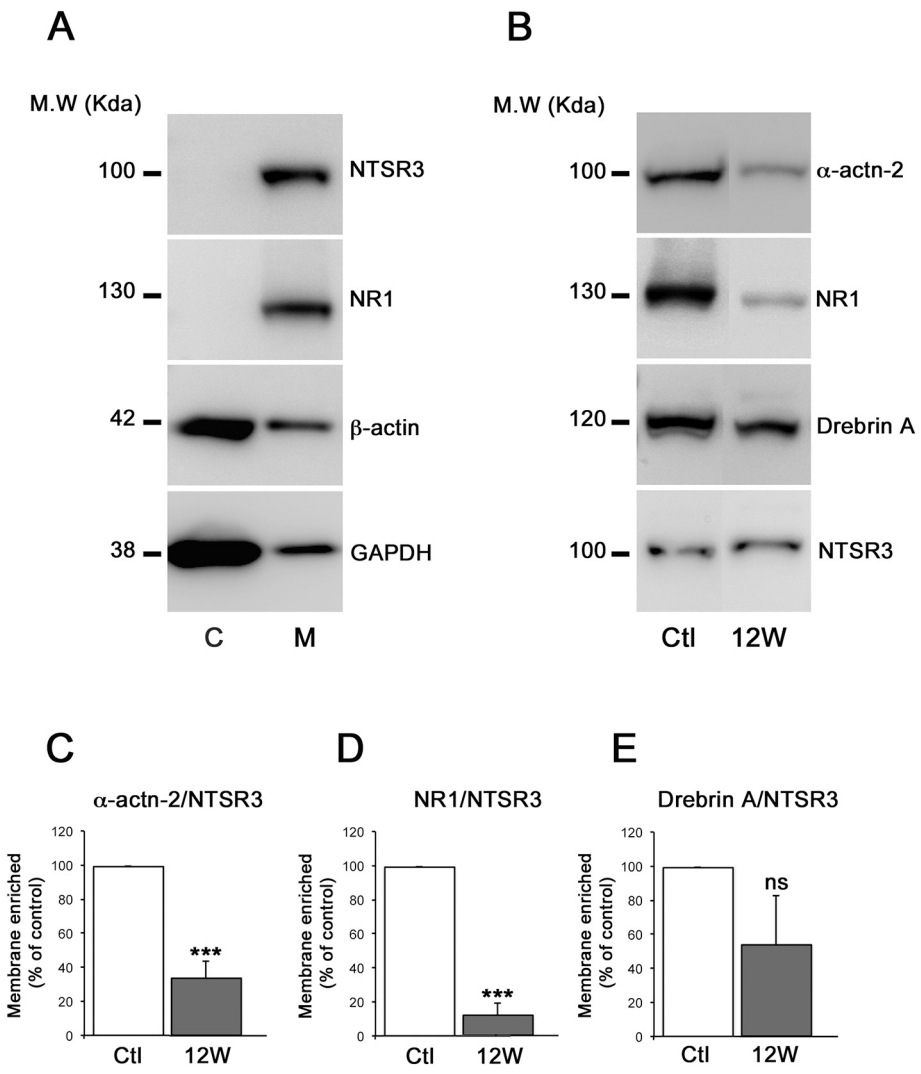


**Fig. 6.** Analysis of the co-regulation of α-actn-2 and NR1 expression levels in Ctl (n=3 rats) and 12 week (n=3 rats) pilocarpine-treated rats. The purity of subcellular fractions from hippocampal tissue isolated from adult rats of 5 months was assessed by Western blotting against specific markers (A). The cytosolic and membrane fractions are denoted by C and M, respectively. Cytosolic markers: β-actin and GAPDH; membrane markers: NR1 and NTSR3. Representative lanes from a Western blot showing NTSR3 (100 kDa), NR1 (130 kDa), β-actin (42 kDa) and GAPDH (38 kDa) protein levels in the hippocampal soluble (lane 1) and membrane fractions (lane 2). B: Representative lanes from a Western blot showing α-actn-2 (100 kDa), NR1, and drebrin A (120 kDa) protein levels in the hippocampal membrane fraction of control (Ctl; lane 1) and pilocarpine rats at 12 weeks (lane 2). NTSR3 is used as a control for normalization of protein loading. Histograms comparing the mean ratios for α-actn-2/NTSR3 (C), NR1/NTSR3 (D), drebrin A/NTSR3 (E) in the hippocampal membrane fraction between Ctl and pilocarpine animals at 12 weeks. The Western blot study shows that the α-actn-2/NTSR3 and NR1/NTSR3 ratios are significantly decreased in pilocarpine animals compared to those of Ctl rats. Note that no significant difference for drebrin A/NTSR3 was found in 12 week pilocarpine animals compared to Ctl rats. Data were converted to percent Ctl for comparison, W, week(s). Statistically significant difference in the mean ratio of labeling is indicated (***$P < 0.001$; ANOVA with a post hoc Student's *t*-test). All data were expressed as the mean ± S.E.M.

the granule cell layer at 2 weeks after pilocarpine treatment and in the hilus at chronic stage (Fig. 2 I). These increases were associated with labeling of numerous cells bodies and processes observed in the granule cell layer and hilus of pilocarpine rats (Fig. 7). Immunolabeling for α-actn-2 in pilocarpine rats was observed within the hilar cells of the dentate gyrus at 12 weeks (Fig. 7B-D) and persisted for up to 16 weeks after SE (Fig. 7E, F). Note that α-actn-2 was found in the cell bodies (Fig. 7B-F, see arrowheads in B, E and F insets) and several processes of these hilar cells were also labeled for α-actn-2 (Fig. 7B-D, F, see arrows in B and F insets).

It has been shown that SE can induce aberrant migration of newly born post-mitotic dentate granule cells from the dentate subgranular zone (SGZ) to the hilus after pilocarpine treatment (Parent et al., 1997; Scharfman et al., 2000; Dashtipour et al., 2001; Parent, 2002; Parent and Lowenstein, 2002; McCloskey et al., 2006; Parent et al., 2006; Parent, 2007; Parent and Murphy, 2008). Indeed, we confirmed in our experimental conditions the increase of numerous ectopic dentate granule cells revealed by Prox-1 (prospero homeobox protein-1) immunolabeling in the hilus of pilocarpine animals (Fig. 8). Figure 8 illustrates Prox-1 immunolabeling in the hippocampal formation of Ctl rats (Fig. 8A, B) and pilocarpine rats at 2 weeks (Fig. 8C, D) and 12 weeks (Fig. 8E, F). In Ctl- and in all pilocarpine rats at all time points examined, Prox-1-immunolabeled cells were densely and uniformely found throughout the granule cell layer (Fig. 8B, D, F). Very few scattered hilar Prox-1-immunolabeled cells were also observed in the hilus (see arrows in Fig. 8B) of Ctl rats consistent with previous work (Amaral, 1978; Seress and Pokorny, 1981; Gaarskjaer and Laurberg, 1983; Martí-Subirana et al., 1986; Scharfman et al., 2003; McCloskey et al., 2006; Parent et al., 2006; Parent, 2007). In contrast with Ctl rats, more hilar Prox-1-immunolabeled cells were distributed throughout the hilus of pilocarpine rats (see arrows in Fig. 8D, F). Thus, our results indicated that Prox-1 is a valid marker to identify the granule cells including ectopic ones within the hilus in our experimental model conditions. Our quantitative data showed that the average number of Prox-1-labeled cells in the hilus after status epilepticus was significantly increased (2 weeks: 163.50 ± 38.55 cells; 7,43 fold; 12 weeks: 170.75 ± 9.94 cells; 7,76 fold; $P < 0.01$; Tukey's test) compared to that of Ctl rats (22 ± 5.13 cells) (Fig. 8G). The average number of ectopic hilar granule cells was stable over time. No statistical difference was found between the average number of Prox-1-labeled cells in the hilus of pilocarpine animals at 2 weeks (163.50 ± 38.55 cells) and 12 weeks (170.75 ± 9.94 cells; $P > 0.05$; ANOVA) (Fig. 8G). Taken together, these data are consistent with those previously reported (McCloskey et al., 2006; Parent et al., 2006; Jiao and Nadler, 2007).

We further examined whether these numerous strongly labeled cells for α-actn-2 within the granule cell layer and hilus could correspond to these ectopic granule cells. Simultaneous detection of α-actn-2 (red) and Prox-1 (green) in Ctl and pilocarpine-treated animals (Fig. 9) revealed that all Prox-1 containing cells were co-labeled with α-actn-2 in the granule cell layer of Ctl (Fig. 9A, B, C) and pilocarpine rats at 2 weeks

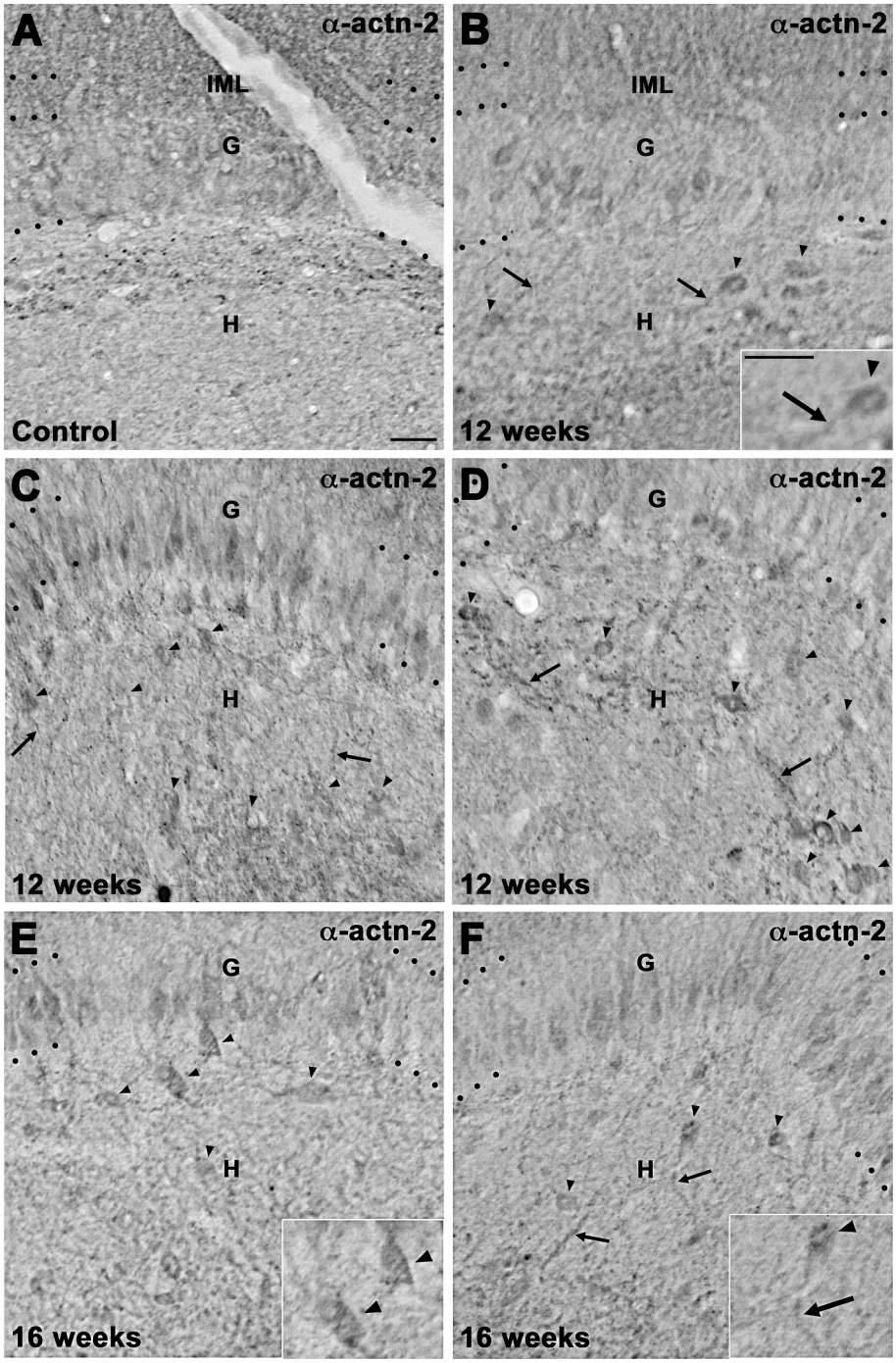


**Fig. 7.** Status epilepticus induces the appearance of hilar α-actn-2 expressing cells in chronic rats. Immunohistochemistry for α-actn-2 in control (Ctl; n= 6 rats; A) and pilocarpine rats at 12 weeks (n= 4 rats; B-D) and 16 weeks (n= 3 rats; E and F). Increased immunolabeling for α-actn-2 in pilocarpine rats was observed within the hilar cells of the dentate gyrus at 12 weeks (B-D), and persisted for up to 16 weeks (E and F) after SE. These hilar cells likely correspond to hilar ectopic dentate granule cells (insets in B, E and F). Note that α-actn-2 was present in the cell bodies (see arrowheads in B-F and insets in B, E and F) and several processes of these hilar cells were also labeled for α-actn-2 (see arrows in B-D and F, and in insets B and F). Scale bars for all panels and insets : 55 μm.

(Fig. 9D, E, F) and 12 weeks (Fig. 9G, H, I). In addition, all ectopic hilar granule cells labeled for Prox-1 were also labeled for α-actn-2 in pilocarpine rats at 2 weeks (see arrows in Fig. 9D, E, F), 12 weeks (see arrows in Fig. 9G, H, I, J) and 16 weeks (see arrows in Fig. 9K). The average diameter of the cell bodies of these ectopic hilar granule cells labeled for α-actn-2 was around 15 μm (n= 10 neurons), consistent with the range of 7-20 μm diameter described previously for these cells (Jiao and Nadler, 2007; Hosford et al., 2016).

At higher magnification, the pattern of α-actn-2 immunolabeling in the somatodendritic compartment (Fig. 9J, K) of ectopic hilar granule cells in chronic rats was punctiform, similar to that previously described *in vivo* (Wyszynski et al., 1998) and *in vitro* (Wyszynski et al., 1997, 1998; Nakagawa et al., 2004; Hodges et al., 2014). Double immunostaining with α-actn-2 and Prox-1 showed that α-actn-2 puncta (red) appeared to be attached to dendritic shafts and were contained in protrusions of different morphology, displaying both large and small heads reminiscent of dendritic spines (see arrowheads in Fig. 9J and inset in Fig. 9K, red).

Thus, our results demonstrate that ectopic spiny granule cells (Pierce et al., 2011) within the hilus of pilocarpine-treated animals express α-actn-2.

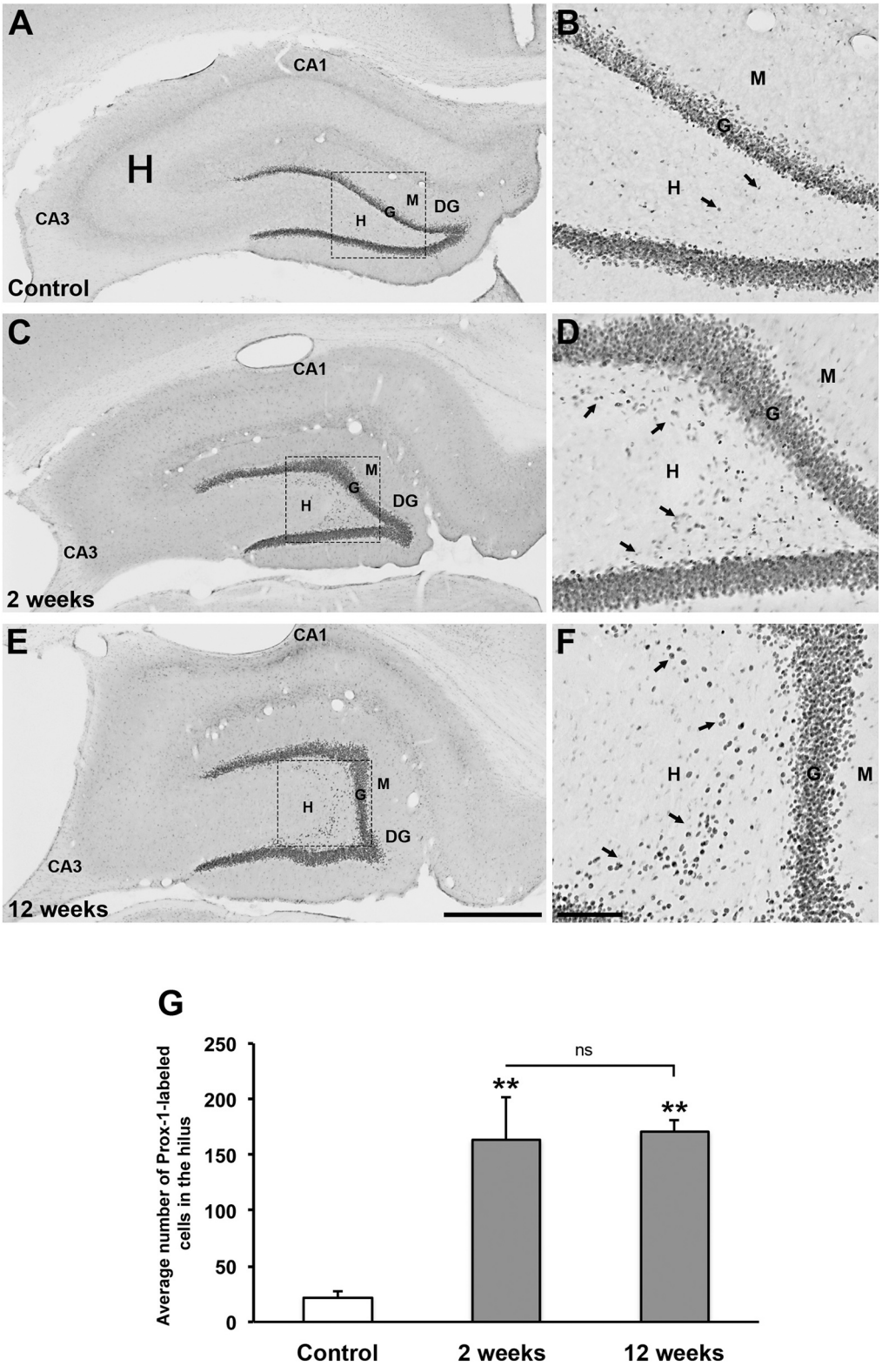


**Fig. 8.** Comparison of immunolabeling for Prox-1 in coronal sections of the hippocampal formation from control (Ctl; n= 3 rats; A and B) and pilocarpine animals at 2 weeks (n= 4 rats; C and D), and 12 weeks (chronic; n= 4 rats; E and F). B, D, and F correspond to higher magnification of boxed dentate gyrus (DG). In Ctl rat (A and B), Prox-1 protein expression is mainly restricted to the granule cell layer (G) of dentate gyrus. Note that very few cells express Prox-1 protein in the hilus (H) of Ctl animals (see arrows). At 2- (C and D) and 12 weeks (E and F) after SE, Prox-1 protein expression is observed in the granule cell layer of dentate gyrus as well as in hilar cells (see arrows). Histogram comparing the average number of Prox-1-labeled cells in the hilus of the dentate gyrus from Ctl and pilocarpine animals at 2- and 12 weeks (G). The mean number of hilar Prox-1 positive cells is significantly increased in pilocarpine animals at 2- and 12 weeks compared with Ctl animals. Scale bars : 500 μm in (A, C and E); 125 μm in (B, D and F).

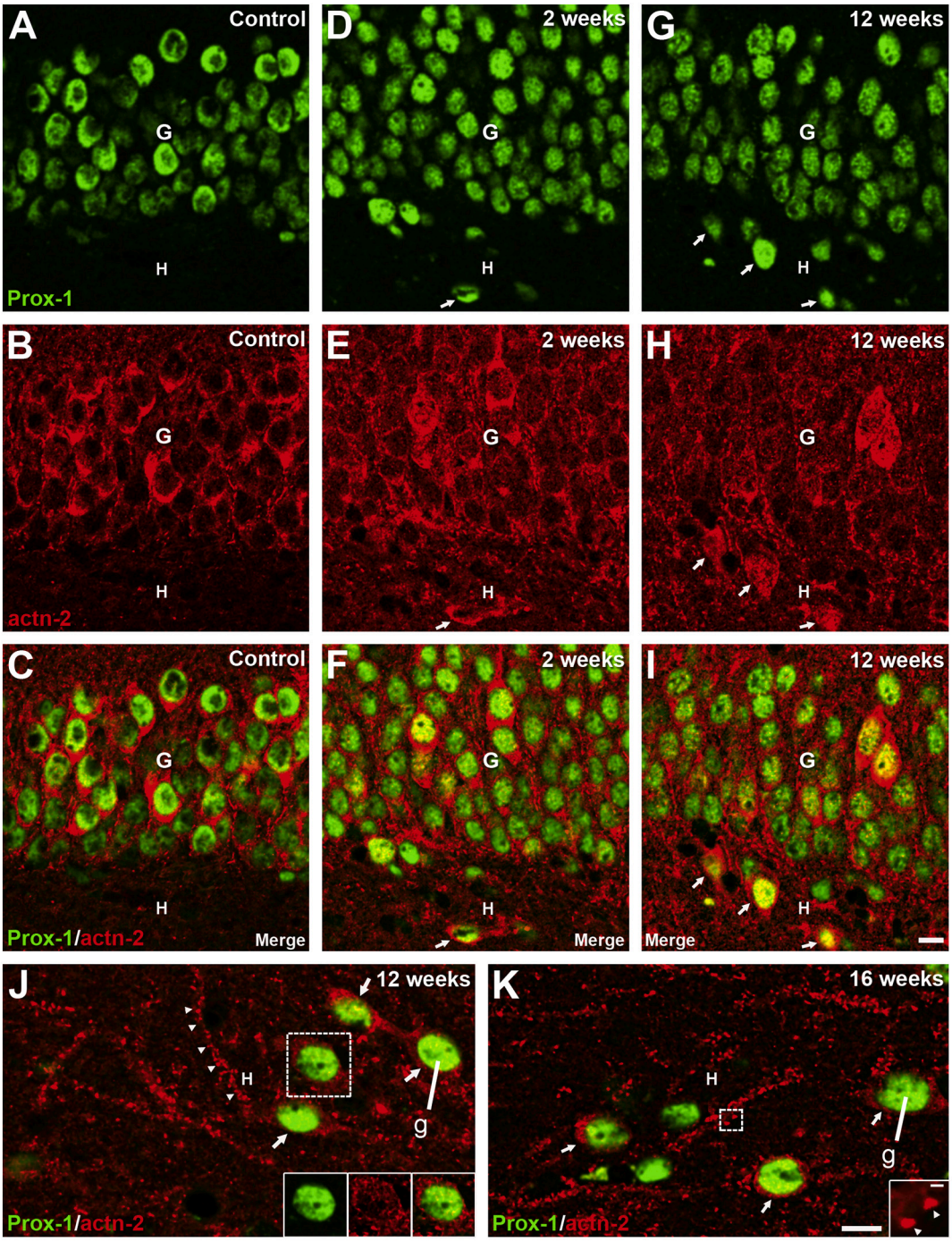


**Fig. 9.** The increased immunolabeling for α-actn-2 in the hilus at chronic stage occurred in the hilar ectopic dentate granule cells. Confocal images of double labeling for Prox-1 (transcription factor, the prospero-like homeobox protein 1, A, D and G, green) and α-actn-2 (B, E and H, red) in coronal sections of dentate gyrus (DG) from control (Ctl; n= 4 rats; A, B and C) and pilocarpine animals at 2- (n= 4 rats; D, E and F) and 12 weeks (n= 4 rats; G, H and I). C, F and I correspond to the merge of panels A and B, D and E, and G and H respectively. In Ctl and pilocarpine animals, the granule cell layer (G) of the dentate gyrus is double-immunolabeled for Prox-1 and α-actn-2 (C, F and I). In addition to this granule cell layer of the dentate gyrus, double-labeled cells for Prox-1 and α-actn-2 are also observed in the hilus (H) of pilocarpine animals (F and I). High magnification images show double-immunolabeled cells (g) for Prox-1 and α-actn-2 in the hilus (J and K, see arrows), which likely correspond to ectopic hilar granule cells. The immunolabeling for α-actn-2 (red) is mainly punctiform in the cell bodies (see arrows in J and K, and see insets in J) and dendrites of ectopic hilar granule cells of chronic pilocarpine rats (J and K), and α-actn-2 puncta appeared in dendritic protrusions (see arrowheads in J and in inset in K, red). Scale bars : 15 μm in A-K and in insets in J; 1μm in inset in K.

## 4. Discussion

### *4.1. Regulation of α-actn-2 expression is associated with neuroplastic modifications observed in pilocarpine rats*

In the pilocarpine model of TLE, we report a significant decrease in α-actn-2 protein levels in the inner molecular layer of the dentate gyrus, the area of major network remodeling. Decreased α-actn-2 protein levels was observed mainly at 1 and 2 weeks after injection of pilocarpine, when sprouting of mossy fibers starts in the supragranular layer of the dentate gyrus (Merrill et al., 2007; Mello et al., 1993; Buckmaster et al., 2002; Longo et al., 2003). At the chronic stage, when the sprouting of

mossy fibers attained a plateau, the α-actn-2 levels in the inner molecular layer were still decreased compared to those in Ctl rats. These observations suggest that α-actn-2 does not play a role in the stabilization of newly formed connections. In addition, this decrease occurred during remodeling of the shape and density of granule cell dendritic spines (Isokawa, 1998, 2000). Double immunostaining studies revealed that α-actn-2 labeled cells in the hilus were also labeled for Prox-1 in pilocarpine animals, confirming that they are newly born migrating granule cells. Altogether, our results suggest that α-actn-2 is not critical in the stabilization and structural integrity of dendritic spines of hippocampal granule cells at chronic stage but its expression is associated with the plasticity of dendritic spines, likely via modulation of the organization and dynamics of actin cytoskeleton.

### 4.2. *α-actn-2 expression is associated with spinogenesis and morphogenesis*

In the inner molecular layer, the dendrites of the dentate granule cells exhibit a global spine loss straightway after pilocarpine-induced SE (Isokawa and Mello, 1991; Isokawa, 1998, 2000). This spine loss arises from denervation of the dendrites of granule cells caused by the death of mossy cells and the degeneration of their axon terminals (Buckmaster et al., 2002; Boulland et al., 2007). Moreover, the loss of dendritic spines found in the inner molecular layer is transitory. A recovery of the spine density started 3 days after SE, reaching a plateau at the chronic phase, 15-35 days later. However, these spine densities never attained Ctl values (Isokawa, 1998, 2000). Remarkably, the recovery rate of spine density is dependent on spine morphology. Indeed, the density of spines with mushroom-shape recovered slowly and incompletely compared to the recovery of thin spines with a clear neck (Isokawa, 1998, 2000). The subsequent recovery of dendritic spine density and shape presumably reflects the development and morphogenesis of new spines on pre-existing granule cell dendrites and/or on outgrowing dendrites from newly born granule cells following epilepsy-induced neurogenesis (Parent et al., 1997; Covolan et al., 2000; Parent, 2002; Parent et al., 2006; Parent, 2007). Based on our results, spine loss is associated with decreased α-actn-2 immunolabeling observed in the inner molecular layer 1 and 2 weeks after pilocarpine injection (see Figure 2), when spinogenesis and spine morphogenesis occur. This observation is in keeping with the work of Hodges et al. (2014), showing that <<α-actn-2 knockdown in rat hippocampal neurons creates an increased density of immature, filopodia-like protrusions that fail to mature into a mushroom-shaped spine during development>>. Therefore, our data suggest that α-actn-2 expression is associated with spinogenesis and morphogenesis of new dendritic spines in the epilepsy model we studied. In addition to α-actn-2, other actin-binding proteins such as actin crosslinker protein spinophilin/neurabin II may also contribute to these functions. In favor of this hypothesis, the work of Feng et al. (2000), whom reported similar observations, showing that Knockout of the spinophilin/neurabin II gene increased the number of filopodia-like protrusions in cultured neurons and the density of spines *in vivo*.

The α-actn-2 protein levels in the inner molecular layer did not return to the Ctl levels at chronic stage, when functional glutamatergic synapses are established (Okazaki et al., 1995; Okazaki and Nadler, 2001; Buckmaster et al., 2002). This strongly suggests that α-actn-2 is not critical for the stabilization and structural integrity of dendritic spines of dentate granule cells. Several lines of evidence support this idea: (1) it has been previously shown that <<α-actin-2 associates and dissociates from post-synaptic sites more dynamically than PSD-95, which appears to be relatively stably integrated in the PSD>> (Nakagawa et al., 2004, 2) our data showed that overexpression of α-actn-2 in CHO-K1 cells did not protect actin filaments from cytochalasin B destabilization, in contrast to other actin-binding proteins such as acidic calponin (Rami et al., 2006) and DA (Ivanov et al., 2009a, 2009b; Ferhat, 2012); (3) similar to non-neuronal cells, it has been reported in cultured hippocampal neurons, that latrunculine A treatment led to a complete loss of α-actn-2 clusters (Allison et al., 1998, 2000), consistent with the fact that α-actn-2 does not stabilize the actin cytoskeleton; (4) the main effect of α-actinins is to organize actin filaments *in vitro*, in non-neuronal cells (Meyer and Aebi, 1990), in various cellular compartments, such as stress fibers (Burridge and Wittchen, 2013), the lamellipodia of migrating cells (Small et al., 2002), cell matrix adhesions (Choi et al., 2008), cadherin-based cell-cell junctions (Knudsen et al., 1995), glomerular podocytes (Dandapani et al., 2007) and in dendritic spines. Indeed, knockdown of α-actn-2 in cultured hippocampal neurons induced decreased actin filament bundles in their dendritic spines (Hodges et al., 2014). Altogether, these observations suggest that the absence of α-actn-2 may affect the dynamics and organization of actin filaments, leading to the plasticity (density and shape) of dendritic spine after SE. These data indicate also that a fine balance of actin filament bundling within the spine is required to drive dendritic spine maturation, density and morphology.

Despite an increase of α-actn-2 mRNA in the granule cell layer at 1-2 weeks after pilocarpine injection, we did not observe a recovery of α-actn-2 protein expression in the inner molecular layer at the chronic stage. At least two possibilities may be considered. The first possibility is that the lack of recovery of actn-2 protein in the inner molecular layer at chronic stage to Ctl levels may be due to the recovery of DA, a stabilizing actin-binding protein at this stage (Ivanov et al., 2009a, 2009b; Ferhat, 2012; Sbai et al., 2012), which is known to inhibit the actin-binding and actin crosslinking activities of α-actinin *in vitro* (Ishikawa et al., 1994). This idea is supported by our data showing that DA-GFP overexpression caused the release of α-actn-2 from F-actin in CHO cells (see Figure 4) and mature cultured hippocampal neurons (see Figure 5). The second possibility is that α-actn-2 mRNA is not translated into α-actn-2 protein within the granule cell bodies leading to reduction levels in the inner molecular layer. This suggestion is unlikely since the increase of α-actn-2 mRNA in the granule cell layer observed at 1-2 weeks after pilocarpine treatment is followed by increased α-actn-2 protein expression in the granule cell layer at 2 weeks after SE. In addition to the reduction α-actn-2 protein expression in inner molecular layer at 1-2 weeks after pilocarpine injection, decreased α-actn-2 mRNA and protein levels were also observed in the hilus. Loss of hilar neurons including mossy cells and inhibitory interneurons is well established in experimental TLE (Sloviter, 1987; Obenaus et al., 1993; Buckmaster et al., 2002; Boulland et al., 2007; Houser, 2014). Therefore, their degeneration is likely to account for the reduction of α-actn-2 expression. In favor of this idea, it has been shown that α-actn-2 is expressed in hilar interneurons (Ratzliff and Soltesz, 2001).

Two hypotheses can be proposed to explain the loss of α-actn-2 in pilocarpine rats at latent stage. First, the decreased levels of α-actn-2 protein in the inner molecular layer of pilocarpine rats may result from the down-regulation of its mRNA expression. Our data argue against this hypothesis. Indeed, the levels of α-actn-2 mRNA were increased compared to those of Ctl rats, in the soma of granule cells. Second, α-actinin has been identified as a substrate of caspase-3, caspase 6 and calpain 1 (Selliah et al., 1996; Raynaud et al., 2003; Lebart and Benyamin, 2006), which are all activated in epilepsy (Ferrer et al., 2000; Henshall et al., 2002; Troy et al., 2002; Narkilahti and Pitkänen, 2005; Seinfeld et al., 2016). Caspase- and/or calpain-mediated actinin breakdown may thus contribute to decrease α-actn-2 immunolabeling in spines located in the inner molecular layer after SE or after DA-GFP overexpression in neurons. Overall, the alteration of the actin cytoskeleton dynamics in dendrites can contribute in dendritic injury and α-actn-2 loss in the inner molecular layer of pilocarpine animals leading to synaptic dysfunction in epilepsy.

### 4.3. *NR1-α-actn-2 co-down-regulation could contribute to synaptic dysfunction in epilepsy*

NR1 expression is down-regulated in the rat pilocarpine model of TLE (Hoeller et al., 2016). In addition, Hodges et al. (2014) have shown

that knocking-down α-actn-2 prevents the recruitment of the NR1 subunit of NMDA receptor to the dendritic spines. Our data in pilocarpine epileptic rats further demonstrate that membrane NR1 is co-down-regulated with membrane α-actn-2. If the effects observed on α-actn-2 and NR1 were due to neuronal loss and/or synapses at chronic stage, the expression of NTSR3 would also be reduced. This is not the case, since our results clearly show that the expression of NTSR3 is not altered at the chronic stage. In conclusion, all these data are in favor of protein regulation of NR1 and α-actn-2 instead of protein loss due to general loss of neuron and/or synapses at this stage. Therefore, the co-down-regulation suggests that the loss of NR1 at the membranes could result from the reduced expression of α-actn-2 in epileptic animals.

Krupp et al. (1999) and Merrill et al. (2007) proposed a model for the interaction between NR1, F-actin and α-actinin. Under resting conditions, NR1 is connected to F-actin via α-actinin. Upon activation of NR1 and the subsequent Ca2+ influx, calmodulin (CaM) is activated (Ca2+/CaM) leading to dissociation of α-actinin from NR1, likely by competitive displacement, resulting in the dissociation of F-actin from NR1. It has been shown by biochemical studies that the levels of drebrin modulate the interaction of α-actinin with F-actin since the actin-binding activity of α-actinin is inhibited by drebrin (Ishikawa et al., 1994). Our data further support such interaction at the cellular level (see Figures 4 and 5). Indeed, we showed that in mature hippocampal neurons DA-GFP overexpression causes significant reduction of α-actn-2 protein in dendritic spines. It is tempting to speculate that the level of DA at the chronic stage is high enough to cause α-actn-2 dissociation from F-actin. Indeed, our data showed that DA expression levels are not modified at chronic stage as compared with Ctl levels (see Figure 6E; Ferhat, 2012; Sbai et al., 2012). If the cytoplasmic domain of NR1 is no more anchored to F-actin and if α-actn-2 dissociated from F-actin, these proteins may be proteolytically cleaved by proteases such as thrombin for NR1 (Gingrich et al., 2000) and caspases and/or calpains for α-actn-2 (Selliah et al., 1996; Ferrer et al., 2000; Communal et al., 2002; Henshall et al., 2002; Troy et al., 2002; Raynaud et al., 2003; Narkilahti and Pitkänen, 2005; Lebart and Benyamin, 2006; Klaiman et al., 2008; Seinfeld et al., 2016; Deng et al., 2019). Obviously, such molecular mechanisms can take place to contribute to α-actn-2 and NR1 loss in hippocampal dendritic spines of pilocarpine-treated animals. Thus, we conclude that in pathological conditions such as epilepsy, the alteration of NR1 anchoring at the membrane of dendritic spines could result from the dissociation of α-actn-2 from F-actin by DA. This alteration of actin cytoskeleton dynamics and organization in dendritic spines could contribute to synaptic dysfunction in epilepsy.

### 4.4. α-actn-2 expression is associated with migrating dentate granule cells

Neurogenesis of granule cells in the dentate gyrus continues throughout life and under physiological conditions, it gives rise to granule cells that migrate from the subgranular zone (SGZ) to the granule cell layer. Dentate granule cell neurogenesis increases greatly after epileptogenic insults (Parent and Lowenstein, 2002). The dentate granule cell layer is often abnormal both in human and experimental TLE, with dispersion of the layer and appearance of hilar-ectopic dentate granule cells (Houser, 1990; Parent and Lowenstein, 2002; McCloskey et al., 2006; Parent et al., 2006; Parent, 2007). These hilar cells arise from neuroblasts of the dentate SGZ origin (Parent et al., 2006), which migrate away from the granule cell layer into the hilus (Parent et al., 1997; Scharfman et al., 2000; Dashtipour et al., 2001; Bonde et al., 2006; Parent et al., 2006). Our data show significantly increased immunolabeling for α-actn-2 in the granule cells of the SGZ 2 weeks after pilocarpine treatment (see Figures 2F and 2I) and this increase is observed in the hilus only at chronic stage (see Figure 2I and Figure 7). One possible explanation is that SE induces increased of α-actn-2 expression in these neuroblasts, which migrate from the dentate SGZ to the hilus of chronic rats 2 weeks after pilocarpine treatment. Indeed, our data showed clearly that the increased immunolabeling for α-actn-2 in the SGZ and the hilus occurred within granule cells of the SGZ and in ectopic granule cells since all α-actn-2 positive cells are also positive for Prox-1. Moreover, increased α-actn-2 was observed during a period of important dentate granule cell migration (Parent et al., 1997, 2006). Several studies reported that the actin cytoskeleton and its associated proteins are instrumental for cell migration (Fox and Walsh, 1999; Ridley et al., 2003; Rottner and Stradal, 2011; Raftopoulou and Hall, 2004; Govek et al., 2005; Broussard et al., 2008; Lian and Sheen, 2015). For example, α-actinin-4, a member of the family of actin-crosslinking proteins, is involved in neural stem/progenitor cell migration (Ge et al., 2016) and in various cancer cell migration and metastasis (Shao et al., 2010, 2014; Lian and Sheen, 2015; Kovac et al., 2018). Thus, α-actn-2 may also play a role in dentate granule cell migration. Further studies are needed to decipher the molecular mechanisms leading to α-actn-2 increase in migrating granule cells. Indeed, the effects of α-actn-2 loss of function *in vivo* need to be determined. However, an RNA interference approach or genetic manipulation may be hampered by the functional redundancy between the related genes of the α-actinin family, three of which (α-actn-1, 2, 4) were found in the PSD fraction (Peng et al., 2004).

### 4.5. Experimental limitations

In the present study, histochemical (immunohistochemistry and *in situ* hybridization) and biochemical analyses were performed on 2 different cohorts. For optimal experimental conditions these 2 approaches cannot be performed using the same animals because the tissues require different treatments (see Material and methods). It has been well-reported that several factors and experimental conditions such as rodent species, strain, sex, age, doses and routes of administration of pilocarpine, as well as combinations with other drugs administered before and/or after SE can affect the severity and the duration of the SE, animal mortality, and therefore potential variability of results between laboratories. Differences between experimental protocoles can lead to variability in the duration of the latent phase, in the frequency and severity of SRS, and in the extent of the lesions including hippocampal and extrahippocampal damage (for review see Curia et al., 2008; Kandratavicius et al., 2014). To limit and overcome variability, methodological procedures should be standardized. Improvement can include continuous EEG video-recordings (Goffin et al., 2007; Sloviter et al., 2007; Curia et al., 2008; Bajorat et al., 2011) to monitor the duration of SE and of the latent period and SRS frequency of each animal. In the present study, using daily visual observations, all pilocarpine animals displayed an average of 4 seizures per day in the two cohorts, as reported by Bajorat et al. (2011). The severity of the SE and SRS could indeed lead to certain variability in the extent of lesions and reorganization of the neuronal networks. However, plasticity of the DG glutamatergic granule cells including spine loss, spinogenesis, morphogenesis, neo-synaptogenesis, aberrant migration, and alterations of NMDA receptors have been well characterized and reproduced by several laboratories using similar pilocarpine models (Isokawa and Mello, 1991; Parent et al., 1997; Isokawa, 1998; Covolan et al., 2000; Isokawa, 2000; Parent, 2002; Parent et al., 2006; Parent, 2007; Kurz et al., 2008; Sbai et al., 2012; Hoeller et al., 2016). Revisiting for example the question of ectopic cell migration in this model (see Figure 8), our results are consistent with previous reports on this issue (Parent et al., 1997, 2006) using different cohorts. Therefore, we emphasize that using the same experimental protocol we can generate animals with relatively similar features allowing to compare data between different cohorts.

## 5. Conclusions

Based on our observations, we conclude that *in vivo,* α-actn-2, together with other proteins such as acidic calponin, is not critical for synaptic structural integrity and stabilization. Indeed, the decreased α-actn-2 protein expression takes place when dentate granule cell spinogenesis and morphogenesis occur. In addition, double

immunostaining studies suggested that the increased α-actn-2 levels in the hilus at chronic stage occurred within migrating granule cells. These effects are likely mediated via modulation of actin cytoskeleton reorganization and dynamics, and glutamatergic synaptic function underlying the development of spontaneous seizures in pilocarpine animals. Thus, α-actn-2 appears as a novel modulator of reactive synaptic and non-synaptic plasticity associated with epilepsy.

## Declaration of Competing Interest

The authors declare no competing interests.

## Acknowledgements

This work was supported by funding from the Centre National de la Recherche Scientifique (CNRS) to the Institut of NeuroPhysiopathologie (INP), UMR7051; the Institut National de la Santé et de la Recherche Médicale (INSERM) to the Institut de Neurosciences des Systèmes (INS) and Aix-Marseille University (AMU) to INS and INP. We thank Dr. Phillipe Benech for reviewing the manuscript and providing valuable comments.

## References

Allison, D.W., Gelfand, V.I., Spector, I., Craig, A.M., 1998. Role of actin in anchoring postsynaptic receptors in cultured hippocampal neurons: differential attachment of NMDA versus AMPA receptors. J. Neurosci. 18, 2423–2436. https://doi.org/10.1523/JNEUROSCI.18-07-02423.1998.

Allison, D.W., Chervin, A.S., Gelfand, V.I., Craig, A.M., 2000. Postsynaptic scaffolds of excitatory and inhibitory synapses in hippocampal neurons: maintenance of core components independent of actin filaments and microtubules. J. Neurosci. 20, 4545–4554. https://doi.org/10.1523/JNEUROSCI.20-12-04545.2000.

Amakhin, D.V., Malkin, S.L., Ergina, J.L., Kryukov, K.A., Veniaminova, E.A., Zubareva, O.E., Zaitsev, A.V., 2017. Alterations in properties of glutamatergic transmission in the temporal cortex and hippocampus following pilocarpine-induced acute seizures in wistar rats. Front. Cell. Neurosci. 11, 264. https://doi.org/10.3389/fncel.2017.00264.

Amaral, D.G., 1978. A Golgi study of cell types in the hilar region of the hippocampus in the rat. J. Comp. Neurol. 182, 851–914. https://doi.org/10.1002/cne.901820508.

Baghirova, S., Hughes, B.G., Hendzel, M.J., Schulz, R., 2015. Sequential fractionation and isolation of subcellular proteins from tissue or cultured cells. MethodsX 2, 440–445. https://doi.org/10.1016/j.mex.2015.11.001.

Bajorat, R., Wilde, M., Sellmann, T., Kirschstein, T., Köhling, R., 2011. Seizure frequency in pilocarpine-treated rats is independent of circadian rhythm. Epilepsia 52, e118–e122. https://doi.org/10.1111/j.1528-1167.2011.03200.x. Epub 2011 Jul 29.

Ballestrem, C., Wehrle-Haller, B., Imhof, B.A., 1998. Actin dynamics in living mammalian cells. J. Cell Sci. 111, 1649–1658.

Barker-Haliski, M., White, H.S., 2015. Glutamatergic mechanisms associated with seizures and epilepsy. Cold Spring Harb. Perspect. Med. 5, a022863. https://doi.org/10.1101/cshperspect.a022863.

Béraud-Dufour, S., Coppola, T., Massa, F., Mazella, J., 2009. Neurotensin receptor-2 and -3 are crucial for the anti-apoptotic effect of neurotensin on pancreatic beta-TC3 cells. Int. J. Biochem. Cell Biol. 41, 2398–2402. https://doi.org/10.1016/j.biocel.2009.04.002.

Bertling, E., Hotulainen, P., 2017. New waves in dendritic spine actin cytoskeleton: From branches and bundles to rings, from actin binding proteins to post-translational modifications. Mol. Cell. Neurosci. 84, 77–84. https://doi.org/10.1016/j.mcn.2017.05.002.

Biou, V., Brinkhaus, H., Malenka, R.C., Matus, A., 2008. Interactions between drebrin and Ras regulate dendritic spine plasticity. Eur. J. Neurosci. 27, 2847–2859. https://doi.org/10.1111/j.1460-9568.2008.06269.x.

Bonde, S., Ekdahl, C.T., Lindvall, O., 2006. Long-term neuronal replacement in adult rat hippocampus after status epilepticus despite chronic inflammation. Eur. J. Neurosci. 23, 965–974. https://doi.org/10.1111/j.1460-9568.2006.04635.x.

Borovac, J., Bosch, M., Okamoto, K., 2018. Regulation of actin dynamics during structural plasticity of dendritic spines: Signaling messengers and actin-binding proteins. Mol. Cell. Neurosci. 91, 122–130. https://doi.org/10.1016/j.mcn.2018.07.001.

Boulland, J.-L., Ferhat, L., Tallak Solbu, T., Ferrand, N., Chaudhry, F.A., Storm-Mathisen, J., Esclapez, M., 2007. Changes in vesicular transporters for gamma-aminobutyric acid and glutamate reveal vulnerability and reorganization of hippocampal neurons following pilocarpine-induced seizures. J. Comp. Neurol. 503, 466–485. https://doi.org/10.1002/cne.21384.

Broussard, J.A., Webb, D.J., Kaverina, I., 2008. Asymmetric focal adhesion disassembly in motile cells. Curr. Opin. Cell Biol. 20, 85–90. https://doi.org/10.1016/j.ceb.2007.10.009.

Buckmaster, P.S., Zhang, G.F., Yamawaki, R., 2002. Axon sprouting in a model of temporal lobe epilepsy creates a predominantly excitatory feedback circuit. J. Neurosci. 22, 6650–6658, 20026730.

Burridge, K., Wittchen, E.S., 2013. The tension mounts: stress fibers as force-generating mechanotransducers. J. Cell Biol. 200, 9–19. https://doi.org/10.1083/jcb.201210090.

Choi, C.K., Vicente-Manzanares, M., Zareno, J., Whitmore, L.A., Mogilner, A., Horwitz, A.R., 2008. Actin and alpha-actinin orchestrate the assembly and maturation of nascent adhesions in a myosin II motor-independent manner. Nat. Cell Biol. 10, 1039–1050. https://doi.org/10.1038/ncb1763.

Communal, C., Sumandea, M., de Tombe, P., Narula, J., Solaro, R.J., Hajjar, R.J., 2002. Functional consequences of caspase activation in cardiac myocytes. Proc. Natl. Acad. Sci. U. S. A. 99, 6252–6256. https://doi.org/10.1073/pnas.092022999.

Cooper, J.A., 1987. Effects of cytochalasin and phalloidin on actin. J. Cell Biol. 105, 1473–1478. https://doi.org/10.1083/jcb.105.4.1473.

Costa, M.S., Rocha, J.B.T., Perosa, S.R., Cavalheiro, E.A., Naffah-Mazzacoratti, M. da G., 2004. Pilocarpine-induced status epilepticus increases glutamate release in rat hippocampal synaptosomes. Neurosci. Lett. 356, 41–44. https://doi.org/10.1016/j.neulet.2003.11.019.

Covolan, L., Ribeiro, L.T., Longo, B.M., Mello, L.E., 2000. Cell damage and neurogenesis in the dentate granule cell layer of adult rats after pilocarpine- or kainate-induced status epilepticus. Hippocampus 10, 169–180. https://doi.org/10.1002/(SICI)1098-1063(2000)10:2<169::AID-HIPO6>3.0.CO;2-W.

Curia, G., Longob, D., Biaginib, G., Jonesc, R.S.G., Avoli, M., 2008. The pilocarpine model of temporal lobe epilepsy. J. Neurosci. Methods 172, 143–157. https://doi.org/10.1016/j.jneumeth.2008.04.019.

Dandapani, S.V., Sugimoto, H., Matthews, B.D., Kolb, R.J., Sinha, S., Gerszten, R.E., Zhou, J., Ingber, D.E., Kalluri, R., Pollak, M.R., 2007. Alpha-actinin-4 is required for normal podocyte adhesion. J. Biol. Chem. 282, 467–477. https://doi.org/10.1074/jbc.M605024200.

Dashtipour, K., Tran, P.H., Okazaki, M.M., Nadler, J.V., Ribak, C.E., 2001. Ultrastructural features and synaptic connections of hilar ectopic granule cells in the rat dentate gyrus are different from those of granule cells in the granule cell layer. Brain Res. 890, 261–271. https://doi.org/10.1016/s0006-8993(00)03119-x.

Debski, K.J., Pitkanen, A., Puhakka, N., Bot, A.M., Khurana, I., Harikrishnan, K.N., Ziemann, M., Kaspi, A., El-Osta, A., Lukasiuk, K., Kobow, K., 2016. Etiology matters - Genomic DNA methylation patterns in three rat models of acquired epilepsy. Sci. Rep. 6, 25668. https://doi.org/10.1038/srep25668.

Dell, R.B., Holleran, S., Ramakrishnan, R., 2002. Sample size determination. ILAR J. 43, 207–213. https://doi.org/10.1093/ilar.43.4.207.

Deng, X., Wang, M., Hu, S., Feng, Y., Shao, Y., Xie, Y., Wu, M., Chen, Y., Shi, X., 2019. The Neuroprotective Effect of Astaxanthin on Pilocarpine-Induced Status Epilepticus in Rats. Front. Cell. Neurosci. 13, 123. https://doi.org/10.3389/fncel.2019.00123.

Di Maio, R., Mastroberardino, P.G., Hu, X., Montero, L., Greenamyre, J.T., 2011. Pilocapine alters NMDA receptor expression and function in hippocampal neurons: NADPH oxidase and ERK1/2 mechanisms. Neurobiol. Dis. 42, 482–495. https://doi.org/10.1016/j.nbd.2011.02.012.

Dunah, A.W., Wyszynski, M., Martin, D.M., Sheng, M., Standaert, D.G., 2000. alpha-actinin-2 in rat striatum: localization and interaction with NMDA glutamate receptor subunits. Brain Res. Mol. Brain Res. 79, 77–87. https://doi.org/10.1016/s0169-328x(00)00102-9.

Edson, K., Weisshaar, B., Matus, A., 1993. Actin depolymerisation induces process formation on MAP2-transfected non-neuronal cells. Development 117, 689–700.

Esclapez, M., Houser, C.R., 1999. Up-regulation of GAD65 and GAD67 in remaining hippocampal GABA neurons in a model of temporal lobe epilepsy. J. Comp. Neurol. 412, 488–505.

Esclapez, M., Tillakaratne, N.J., Tobin, A.J., Houser, C.R., 1993. Comparative localization of mRNAs encoding two forms of glutamic acid decarboxylase with nonradioactive in situ hybridization methods. J. Comp. Neurol. 331, 339–362. https://doi.org/10.1002/cne.903310305.

Esclapez, M., Tillakaratne, N.J., Kaufman, D.L., Tobin, A.J., Houser, C.R., 1994. Comparative localization of two forms of glutamic acid decarboxylase and their mRNAs in rat brain supports the concept of functional differences between the forms. J. Neurosci. 14, 1834–1855. https://doi.org/10.1523/JNEUROSCI.14-03-01834.1994.

Esclapez, M., Hirsch, J.C., Ben-Ari, Y., Bernard, C., 1999. Newly formed excitatory pathways provide a substrate for hyperexcitability in experimental temporal lobe epilepsy. J. Comp. Neurol. 408, 449–460.

Feng, J., Yan, Z., Ferreira, A., Tomizawa, K., Liauw, J.A., Zhuo, M., Allen, P.B., Ouimet, C.C., Greengard, P., 2000. Spinophilin regulates the formation and function of dendritic spines. Proc. Natl. Acad. Sci. U. S. A. 97, 9287–9292. https://doi.org/10.1073/pnas.97.16.9287.

Ferhat, L., 2012. Potential role of drebrin a, an f-actin binding protein, in reactive synaptic plasticity after pilocarpine-induced seizures: functional implications in epilepsy. Int. J. Cell Biol. 2012 https://doi.org/10.1155/2012/474351, 474351.

Ferhat, L., Cook, C., Chauviere, M., Harper, M., Kress, M., Lyons, G.E., Baas, P.W., 1998a. Expression of the mitotic motor protein Eg5 in postmitotic neurons: implications for neuronal development. J. Neurosci. 18, 7822–7835. https://doi.org/10.1523/JNEUROSCI.18-19-07822.1998.

Ferhat, L., Kuriyama, R., Lyons, G.E., Micales, B., Baas, P.W., 1998b. Expression of the mitotic motor protein CHO1/MKLP1 in postmitotic neurons. Eur. J. Neurosci. 10, 1383–1393. https://doi.org/10.1046/j.1460-9568.1998.00159.x.

Ferhat, L., Esclapez, M., Represa, A., Fattoum, A., Shirao, T., Ben-Ari, Y., 2003. Increased levels of acidic calponin during dendritic spine plasticity after pilocarpine-induced seizures. Hippocampus 13, 845–858. https://doi.org/10.1002/hipo.10136.

Ferrer, I., López, E., Blanco, R., Rivera, R., Krupinski, J., Martí, E., 2000. Differential c-Fos and caspase expression following kainic acid excitotoxicity. Acta Neuropathol. 99, 245–256. https://doi.org/10.1007/pl00007434.

Festing, M.F.W., Altman, D.G., 2002. Guidelines for the design and statistical analysis of experiments using laboratory animals. ILAR J. 43, 244–258. https://doi.org/10.1093/ilar.43.4.244.

Fox, J.W., Walsh, C.A., 1999. Periventricular heterotopia and the genetics of neuronal migration in the cerebral cortex. Am. J. Hum. Genet. 65, 19–24. https://doi.org/10.1086/302474.

Freund, T.F., Buzsáki, G., 1996. Interneurons of the hippocampus. Hippocampus 6, 347–470. https://doi.org/10.1002/(SICI)1098-1063(1996)6:4<347::AID-HIPO1>3.0.CO;2-I.

Gaarskjaer, F.B., Laurberg, S., 1983. Ectopic granule cells of hilus fasciae dentatae projecting to the ipsilateral regio inferior of the rat hippocampus. Brain Res. 274, 11–16. https://doi.org/10.1016/0006-8993(83)90516-4.

Ge, H., Yu, A., Chen, J., Yuan, J., Yin, Y., Duanmu, W., Tan, L., Yang, Y., Lan, C., Chen, W., Feng, H., Hu, R., 2016. Poly-L-ornithine enhances migration of neural stem/progenitor cells via promoting α-Actinin 4 binding to actin filaments. Sci. Rep. 6, 37681. https://doi.org/10.1038/srep37681.

Geddes, J.W., Cahan, L.D., Cooper, S.M., Kim, R.C., Choi, B.H., Cotman, C.W., 1990. Altered distribution of excitatory amino acid receptors in temporal lobe epilepsy. Exp. Neurol. 108, 214–220. https://doi.org/10.1016/0014-4886(90)90125-c.

Gingrich, M.B., Junge, C.E., Lyuboslavsky, P., Traynelis, S.F., 2000. Potentiation of NMDA receptor function by the serine protease thrombin. J. Neurosci. 20, 4582–4595. https://doi.org/10.1007/978-3-319-45096-4_14.

Goffin, K., Nissinen, J., Van Laere, K., Pitkänen, A., 2007. Cyclicity of spontaneous recurrent seizures in pilocarpine model of temporal lobe epilepsy in rat. J. Exp. Neurol. 205 (2007), 501–505. https://doi.org/10.1016/J.expneurol.2007.03.008.

Govek, E.-E., Newey, S.E., Van Aelst, L., 2005. The role of the Rho GTPases in neuronal development. Genes Dev. 19, 1–49. https://doi.org/10.1101/gad.1256405.

Hall, D.D., Dai, S., Tseng, P.-Y., Malik, Z., Nguyen, M., Matt, L., Schnizler, K., Shephard, A., Mohapatra, D.P., Tsuruta, F., Dolmetsch, R.E., Christel, C.J., Lee, A., Burette, A., Weinberg, R.J., Hell, J.W., 2013. Competition between α-actinin and $Ca^{2+}$-calmodulin controls surface retention of the L-type $Ca^{2+}$ channel Ca(V)1.2. Neuron 78, 483–497. https://doi.org/10.1016/j.neuron.2013.02.032.

Henshall, D.C., Skradski, S.L., Meller, R., Araki, T., Minami, M., Schindler, C.K., Lan, J. Q., Bonislawski, D.P., Simon, R.P., 2002. Expression and differential processing of caspases 6 and 7 in relation to specific epileptiform EEG patterns following limbic seizures. Neurobiol. Dis. 10, 71–87. https://doi.org/10.1006/nbdi.2002.0505.

Henson, M.A., Larsen, R.S., Lawson, S.N., Pérez-Otaño, I., Nakanishi, N., Lipton, S.A., Philpot, B.D., 2012. Genetic deletion of NR3A accelerates glutamatergic synapse maturation. PLoS One 7, e42327. https://doi.org/10.1371/journal.pone.0042327.

Hodges, J.L., Vilchez, S.M., Asmussen, H., Whitmore, L.A., Horwitz, A.R., 2014. α-Actinin-2 mediates spine morphology and assembly of the post-synaptic density in hippocampal neurons. PLoS One 9, e101770. https://doi.org/10.1371/journal.pone.0101770.

Hoe, H.-S., Lee, J.-Y., Pak, D.T.S., 2009. Combinatorial morphogenesis of dendritic spines and filopodia by SPAR and alpha-actinin2. Biochem. Biophys. Res. Commun. 384, 55–60. https://doi.org/10.1016/j.bbrc.2009.04.069.

Hoeller, A.A., Costa, A.P.R., Bicca, M.A., Matheus, F.C., Lach, G., Spiga, F., Lightman, S. L., Walz, R., Collingridge, G.L., Bortolotto, Z.A., de Lima, T.C.M., 2016. The role of hippocampal NMDA receptors in long-term emotional responses following muscarinic receptor activation. PLoS One 11, e0147293. https://doi.org/10.1371/journal.pone.0147293.

Honda, K., 2015. The biological role of actinin-4 (ACTN4) in malignant phenotypes of cancer. Cell Biosci. 5, 41. https://doi.org/10.1186/s13578-015-0031-0.

Hosford, D.A., Crain, B.J., Cao, Z., Bonhaus, D.W., Friedman, A.H., Okazaki, M.M., 1991. Increased AMPA-sensitive quisqualate receptor binding and reduced NMDA receptor binding in epileptic human hippocampus. J. Neurosci. 11 (2), 428–434. https://doi.org/10.1523/JNEUROSCI.11-02-00428.

Hosford, B.E., Liska, J.P., Danzer, S.C., 2016. Ablation of newly generated hippocampal granule cells has disease-modifying effects in epilepsy. J. Neurosci. 36, 11013–11023. https://doi.org/10.1523/JNEUROSCI.1371-16.2016.

Hotulainen, P., Hoogenraad, C.C., 2010. Actin in dendritic spines: connecting dynamics to function. J. Cell Biol. 189, 619–629. https://doi.org/10.1083/jcb.201003008.

Houser, C.R., 1990. Granule cell dispersion in the dentate gyrus of humans with temporal lobe epilepsy. Brain Res. 535, 195–204. https://doi.org/10.1016/0006-8993(90)91601-c.

Houser, C.R., 2007. Interneurons of the dentate gyrus: an overview of cell types, terminal fields and neurochemical identity. Prog. Brain Res. 163, 217–232. https://doi.org/10.1016/S0079-6123(07)63013-1.

Houser, C.R., 2014. Do Structural Changes in GABA Neurons Give Rise to the Epileptic State? Adv. Exp. Med. Biol. 813, 151–160. https://doi.org/10.1007/978-94-017-8914-1_12.

Ishikawa, R., Hayashi, K., Shirao, T., Xue, Y., Takagi, T., Sasaki, Y., Kohama, K., 1994. Drebrin, a development-associated brain protein from rat embryo, causes the dissociation of tropomyosin from actin filaments. J. Biol. Chem. 269, 29928–29933.

Isokawa, M., 1998. Remodeling dendritic spines in the rat pilocarpine model of temporal lobe epilepsy. Neurosci. Lett. 258, 73–76. https://doi.org/10.1016/s0304-3940(98)00848-9.

Isokawa, M., 2000. Remodeling dendritic spines of dentate granule cells in temporal lobe epilepsy patients and the rat pilocarpine model. Epilepsia 41 (Suppl. 6), S14–S17. https://doi.org/10.1111/j.1528-1157.2000.tb01550.x.

Isokawa, M., Mello, L.E., 1991. NMDA receptor-mediated excitability in dendritically deformed dentate granule cells in pilocarpine-treated rats. Neurosci. Lett. 129, 69–73. https://doi.org/10.1016/0304-3940(91)90722-6.

Ivanov, A., Esclapez, M., Ferhat, L., 2009a. Role of drebrin A in dendritic spine plasticity and synaptic function: implications in neurological disorders. Commun. Integr. Biol. 2, 268–270. https://doi.org/10.4161/cib.2.3.8166.

Ivanov, A., Esclapez, M., Pellegrino, C., Shirao, T., Ferhat, L., 2009b. Drebrin A regulates dendritic spine plasticity and synaptic function in mature cultured hippocampal neurons. J. Cell Sci. 122, 524–534. https://doi.org/10.1242/jcs.033464.

Jalan-Sakrikar, N., Bartlett, R.K., Baucum, A.J., Colbran, R.J., 2012. Substrate-selective and calcium-independent activation of CaMKII by α-actinin. J. Biol. Chem. 287, 15275–15283. https://doi.org/10.1074/jbc.M112.351817.

Jiang, Q., Wang, J., Wu, X., Jiang, Y., 2007. Alterations of NR2B and PSD-95 expression after early-life epileptiform discharges in developing neurons. Int. J. Dev. Neurosci. 25, 165–170. https://doi.org/10.1016/j.ijdevneu.2007.02.001.

Jiao, Y., Nadler, J.V., 2007. Stereological analysis of GluR2-immunoreactive hilar neurons in the pilocarpine model of temporal lobe epilepsy: correlation of cell loss with mossy fiber sprouting. Exp. Neurol. 205, 569–582. https://doi.org/10.1016/j.expneurol.2007.03.025.

Kandratavicius, L., Balista, P.A., Lopes-Aguiar, C., Ruggiero, R.N., Umeoka, E.H., Garcia-Cairasco, N., Bueno-Junior, L.S., Leite, J.P., 2014. Animal models of epilepsy: use and limitations. Neuropsychiatric Disease and Treatment 10, 1693–1705. https://doi.org/10.2147/NDT.S50371.

Khan, R., Krishnakumar, A., Paulose, C.S., 2008. Decreased glutamate receptor binding and NMDA R1 gene expression in hippocampus of pilocarpine-induced epileptic rats: neuroprotective role of Bacopa monnieri extract. Epilepsy Behav. 12, 54–60. https://doi.org/10.1016/j.yebeh.2007.09.021.

Klaiman, G., Petzke, T.L., Hammond, J., Leblanc, A.C., 2008. Targets of caspase-6 activity in human neurons and Alzheimer disease. Mol. Cell. Proteomics 1541–1555. https://doi.org/10.1074/mcp.M800007-MCP200.

Knudsen, K.A., Soler, A.P., Johnson, K.R., Wheelock, M.J., 1995. Interaction of alpha-actinin with the cadherin/catenin cell-cell adhesion complex via alpha-catenin. J. Cell Biol. 130, 67–77. https://doi.org/10.1083/jcb.130.1.67.

Koganezawa, N., Hanamura, K., Sekino, Y., Shirao, T., 2017. The role of drebrin in dendritic spines. Mol. Cell. Neurosci. 84, 85–92. https://doi.org/10.1016/j.mcn.2017.01.004.

Kovac, B., Mäkelä, T.P., Vallenius, T., 2018. Increased α-actinin-1 destabilizes E-cadherin-based adhesions and associates with poor prognosis in basal-like breast cancer. PLoS One 13, e0196986. https://doi.org/10.1371/journal.pone.0196986.

Krupp, J.J., Vissel, B., Thomas, C.G., Heinemann, S.F., Westbrook, G.L., 1999. Interactions of calmodulin and alpha-actinin with the NR1 subunit modulate Ca2+-dependent inactivation of NMDA receptors. J. Neurosci. 19, 1165–1178. https://doi.org/10.1523/JNEUROSCI.19-04-01165.1999.

Kurz, J.E., Moore, B.J., Henderson, S.C., Campbell, J.N., Churn, S.B., 2008. A cellular mechanism for dendritic spine loss in the pilocarpine model of status epilepticus. Epilepsia 49, 1696–1710. https://doi.org/10.1111/j.1528-1167.2008.01616.x.

Lai, K.-O., Ip, N.Y., 2013. Structural plasticity of dendritic spines: the underlying mechanisms and its dysregulation in brain disorders. Biochim. Biophys. Acta 1832, 2257–2263. https://doi.org/10.1016/j.bbadis.2013.08.012.

Lebart, M.-C., Benyamin, Y., 2006. Calpain involvement in the remodeling of cytoskeletal anchorage complexes. FEBS J. 273, 3415–3426. https://doi.org/10.1111/j.1742-4658.2006.05350.x.

Lee, S., Miskovsky, J., Williamson, J., Howells, R., Devinsky, O., Lothman, E., Christakos, S., 1994. Changes in glutamate receptor and proenkephalin gene expression after kindled seizures. Brain Res. Mol. Brain Res. 24, 34–42. https://doi.org/10.1016/0169-328x(94)90115-5.

Li, Q., Dai, X.-Q., Shen, P.Y., Wu, Y., Long, W., Chen, C.X., Hussain, Z., Wang, S., Chen, X.-Z., 2007. Direct binding of alpha-actinin enhances TRPP3 channel activity. J. Neurochem. 103, 2391–2400. https://doi.org/10.1111/j.1471-4159.2007.04940.x.

Lian, G., Sheen, V.L., 2015. Cytoskeletal proteins in cortical development and disease: actin associated proteins in periventricular heterotopia. Front. Cell. Neurosci. 9, 99. https://doi.org/10.3389/fncel.2015.00099.

Longo, B., Covolan, L., Chadi, G., Mello, L.E.A.M., 2003. Sprouting of mossy fibers and the vacating of postsynaptic targets in the inner molecular layer of the dentate gyrus. Exp. Neurol. 181, 57–67. https://doi.org/10.1016/s0014-4886(02)00046-8.

Lopes, M.W., Soares, F.M.S., de Mello, N., Nunes, J.C., Cajado, A.G., de Brito, D., de Cordova, F.M., da Cunha, R.M.S., Walz, R., Leal, R.B., 2013. Time-dependent modulation of AMPA receptor phosphorylation and mRNA expression of NMDA receptors and glial glutamate transporters in the rat hippocampus and cerebral cortex in a pilocarpine model of epilepsy. Exp. Brain Res. 226, 153–163. https://doi.org/10.1007/s00221-013-3421-8.

Martí-Subirana, A., Soriano, E., García-Verdugo, J.M., 1986. Morphological aspects of the ectopic granule-like cellular populations in the albino rat hippocampal formation: a Golgi study. J. Anat. 144, 31–47.

Maruoka, N.D., Steele, D.F., Au, B.P., Dan, P., Zhang, X., Moore, E.D., Fedida, D., 2000. alpha-actinin-2 couples to cardiac Kv1.5 channels, regulating current density and channel localization in HEK cells. FEBS Lett. 473, 188–194. https://doi.org/10.1016/s0014-5793(00)01521-0.

Matt, L., Kim, K., Hergarden, A.C., Patriarchi, T., Malik, Z.A., Park, D.K., Chowdhury, D., Buonarati, O.R., Henderson, P.B., Gökçek Saraç, Ç., Zhang, Y., Mohapatra, D., Horne, M.C., Ames, J.B., Hell, J.W., 2018. α-Actinin Anchors PSD-95 at Postsynaptic Sites. Neuron 97, 1094–1109.e9. https://doi.org/10.1016/j.neuron.2018.01.036.

Mazella, J., Pétrault, O., Lucas, G., Deval, E., Béraud-Dufour, S., Gandin, C., El-Yacoubi, M., Widmann, C., Guyon, A., Chevet, E., Taouji, S., Conductier, G., Corinus, A., Coppola, T., Gobbi, G., Nahon, J.-L., Heurteaux, C., Borsotto, M., 2010. Spadin, a sortilin-derived peptide, targeting rodent TREK-1 channels: a new concept in the antidepressant drug design. PLoS Biol. 8, e1000355. https://doi.org/10.1371/journal.pbio.1000355.

McCloskey, D.P., Hintz, T.M., Pierce, J.P., Scharfman, H.E., 2006. Stereological methods reveal the robust size and stability of ectopic hilar granule cells after pilocarpine-

induced status epilepticus in the adult rat. Eur. J. Neurosci. 24, 2203–2210. https://doi.org/10.1111/j.1460-9568.2006.05101.x.
McDonald, J.W., Garofalo, E.A., Hood, T., Sackellares, J.C., Gilman, S., McKeever, P.E., Troncoso, J.C., Johnston, M.V., 1991. Altered excitatory and inhibitory amino acid receptor binding in hippocampus of patients with temporal lobe epilepsy. Ann. Neurol. 29, 529–541. https://doi.org/10.1002/ana.410290513.
Mello, L.E., Cavalheiro, E.A., Tan, A.M., Kupfer, W.R., Pretorius, J.K., Babb, T.L., Finch, D.M., 1993. Circuit mechanisms of seizures in the pilocarpine model of chronic epilepsy: cell loss and mossy fiber sprouting. Epilepsia 34, 985–995. https://doi.org/10.1111/j.1528-1157.1993.tb02123.x.
Merrill, M.A., Malik, Z., Akyol, Z., Bartos, J.A., Leonard, A.S., Hudmon, A., Shea, M.A., Hell, J.W., 2007. Displacement of alpha-actinin from the NMDA receptor NR1 C0 domain By Ca2+/calmodulin promotes CaMKII binding. Biochemistry 46, 8485–8497. https://doi.org/10.1021/bi062302.
Meyer, R.K., Aebi, U., 1990. Bundling of actin filaments by alpha-actinin depends on its molecular length. J. Cell Biol. 110, 2013–2024. https://doi.org/10.1083/jcb.110.6.2013.
Michailidis, I.E., Helton, T.D., Petrou, V.I., Mirshahi, T., Ehlers, M.D., Logothetis, D.E., 2007. Phosphatidylinositol-4,5-bisphosphate regulates NMDA receptor activity through alpha-actinin. J. Neurosci. 27, 5523–5532. https://doi.org/10.1523/JNEUROSCI.4378-06.2007.
Mikati, M.A., Grintsevich, E.E., Reisler, E., 2013. Drebrin-induced stabilization of actin filaments. J. Biol. Chem. 288, 19926–19938. https://doi.org/10.1074/jbc.M113.472647.
Murphy, A.C.H., Young, P.W., 2015. The actinin family of actin cross-linking proteins - a genetic perspective. Cell Biosci. 5, 49. https://doi.org/10.1186/s13578-015-0029-7.
Nakagawa, T., Engler, J.A., Sheng, M., 2004. The dynamic turnover and functional roles of alpha-actinin in dendritic spines. Neuropharmacology 47, 734–745. https://doi.org/10.1016/j.neuropharm.2004.07.022.
Narkilahti, S., Pitkänen, A., 2005. Caspase 6 expression in the rat hippocampus during epileptogenesis and epilepsy. Neuroscience 131, 887–897. https://doi.org/10.1016/j.neuroscience.2004.12.013.
Obenaus, A., Esclapez, M., Houser, C.R., 1993. Loss of glutamate decarboxylase mRNA-containing neurons in the rat dentate gyrus following pilocarpine-induced seizures. J. Neurosci. 13, 4470–4485. https://doi.org/10.1523/JNEUROSCI.13-10-04470.1993.
Okazaki, M.M., Nadler, J.V., 2001. Glutamate receptor involvement in dentate granule cell epileptiform activity evoked by mossy fiber stimulation. Brain Res. 915, 58–69. https://doi.org/10.1016/s0006-8993(01)02824-4.
Okazaki, M.M., Evenson, D.A., Nadler, J.V., 1995. Hippocampal mossy fiber sprouting and synapse formation after status epilepticus in rats: visualization after retrograde transport of biocytin. J. Comp. Neurol. 352, 515–534. https://doi.org/10.1002/cne.903520404.
Otey, C.A., Carpen, O., 2004. Alpha-actinin revisited: a fresh look at an old player. Cell Motil. Cytoskeleton 58, 104–111. https://doi.org/10.1002/cm.20007.
Otey, C.A., Pavalko, F.M., Burridge, K., 1990. An interaction between alpha-actinin and the beta 1 integrin subunit in vitro. J. Cell Biol. 111, 721–729. https://doi.org/10.1083/jcb.111.2.721.
Otey, C.A., Vasquez, G.B., Burridge, K., Erickson, B.W., 1993. Mapping of the alpha-actinin binding site within the beta 1 integrin cytoplasmic domain. J. Biol. Chem. 268, 21193–21197.
Parent, J.M., 2002. The role of seizure-induced neurogenesis in epileptogenesis and brain repair. Epilepsy Res. 50, 179–189. https://doi.org/10.1016/s0920-1211(02)00078-5.
Parent, J.M., 2007. Adult neurogenesis in the intact and epileptic dentate gyrus. Prog. Brain Res. 163, 529–540. https://doi.org/10.1016/S0079-6123(07)63028-3.
Parent, J.M., Lowenstein, D.H., 2002. Seizure-induced neurogenesis: are more new neurons good for an adult brain? Prog. Brain Res. 135, 121–131. https://doi.org/10.1016/S0079-6123(02)35012-X.
Parent, J.M., Murphy, G.G., 2008. Mechanisms and functional significance of aberrant seizure-induced hippocampal neurogenesis. Epilepsia 49 (Suppl. 5), 19–25. https://doi.org/10.1111/j.1528-1167.2008.01634.x.
Parent, J.M., Yu, T.W., Leibowitz, R.T., Geschwind, D.H., Sloviter, R.S., Lowenstein, D. H., 1997. Dentate granule cell neurogenesis is increased by seizures and contributes to aberrant network reorganization in the adult rat hippocampus. J. Neurosci. 17, 3727–3738. https://doi.org/10.1523/JNEUROSCI.17-10-03727.1997.
Parent, J.M., Elliott, R.C., Pleasure, S.J., Barbaro, N.M., Lowenstein, D.H., 2006. Aberrant seizure-induced neurogenesis in experimental temporal lobe epilepsy. Ann. Neurol. 59, 81–91. https://doi.org/10.1002/ana.20699.
Pavalko, F.M., Otey, C.A., Simon, K.O., Burridge, K., 1991. Alpha-actinin: a direct link between actin and integrins. Biochem. Soc. Trans. 19, 1065–1069. https://doi.org/10.1042/bst0191065.
Peng, J., Kim, M.J., Cheng, D., Duong, D.M., Gygi, S.P., Sheng, M., 2004. Semiquantitative proteomic analysis of rat forebrain postsynaptic density fractions by mass spectrometry. J. Biol. Chem. 279, 21003–21011. https://doi.org/10.1074/jbc.M400103200.
Peng, W.-F., Ding, J., Li, X., Fan, F., Zhang, Q.-Q., Wang, X., 2016. N-methyl-D-aspartate receptor NR2B subunit involved in depression-like behaviours in lithium chloride-pilocarpine chronic rat epilepsy model. Epilepsy Res. 119, 77–85. https://doi.org/10.1016/j.eplepsyres.2015.09.013.
Penny, C.J., Gold, M.G., 2018. Mechanisms for localising calcineurin and CaMKII in dendritic spines. Cell. Signal. 49, 46–58. https://doi.org/10.1016/j.cellsig.2018.05.010.
Pierce, J.P., McCloskey, D.P., Scharfman, H.E., 2011. Morphometry of hilar ectopic granule cells in the rat. J. Comp. Neurol. 519, 1196–1218. https://doi.org/10.1002/cne.22568.
Racine, R.J., 1972. Modification of seizure activity by electrical simulation: II. Motor seizure. Electroencephalogr. Clin. Neurophysiol. 32, 281–294. https://doi.org/10.1016/0013-4694(72)90177-0.
Raftopoulou, M., Hall, A., 2004. Cell migration: Rho GTPases lead the way. Dev. Biol. 265, 23–32. https://doi.org/10.1016/j.ydbio.2003.06.003.
Rami, G., Caillard, O., Medina, I., Pellegrino, C., Fattoum, A., Ben-Ari, Y., Ferhat, L., 2006. Change in the shape and density of dendritic spines caused by overexpression of acidic calponin in cultured hippocampal neurons. Hippocampus 16, 183–197. https://doi.org/10.1002/hipo.20145.
Ratzliff, A.D., Soltesz, I., 2001. Differential immunoreactivity for alpha-actinin-2, an N-methyl-D-aspartate-receptor/actin binding protein, in hippocampal interneurons. Neuroscience 103, 337–349. https://doi.org/10.1016/s0306-4522(01)00013-6.
Raynaud, F., Bonnal, C., Fernandez, E., Bremaud, L., Cerutti, M., Lebart, M.-C., Roustan, C., Ouali, A., Benyamin, Y., 2003. The calpain 1-alpha-actinin interaction. Resting complex between the calcium-dependent protease and its target in cytoskeleton. Eur. J. Biochem. 270, 4662–4670. https://doi.org/10.1046/j.1432-1033.2003.03859.x.
Raza, M., Pal, S., Rafiq, A., DeLorenzo, R.J., 2001. Long-term alteration of calcium homeostatic mechanisms in the pilocarpine model of temporal lobe epilepsy. Brain Res. 903, 1–12. https://doi.org/10.1016/s0006-8993(01)02127-8.
Reyes-Montaño, E.A., Lareo, L.R., Chow, D.-C., Pérez-Gómez, G., 2006. Immunolocalization and biochemical characterization of N-methyl-D-aspartate receptor subunit NR1 from rat brain. Protein J. 25, 95–108. https://doi.org/10.1007/s10930-006-0001-9.
Ridley, A.J., Schwartz, M.A., Burridge, K., Firtel, R.A., Ginsberg, M.H., Borisy, G., Parsons, J.T., Horwitz, A.R., 2003. Cell migration: integrating signals from front to back. Science 302, 1704–1709. https://doi.org/10.1126/science.1092053.
Rottner, K., Stradal, T.E.B., 2011. Actin dynamics and turnover in cell motility. Curr. Opin. Cell Biol. 23, 569–578. https://doi.org/10.1016/j.ceb.2011.07.003.
Sadeghi, A., Doyle, A.D., Johnson, B.D., 2002. Regulation of the cardiac L-type Ca2+ channel by the actin-binding proteins alpha-actinin and dystrophin. Am. J. Phys. Cell Physiol. 282, C1502–C1511. https://doi.org/10.1152/ajpcell.00435.2001.
Sbai, O., Khrestchatisky, M., Esclapez, M., Ferhat, L., 2012. Drebrin A expression is altered after pilocarpine-induced seizures: time course of changes is consistent for a role in the integrity and stability of dendritic spines of hippocampal granule cells. Hippocampus 22, 477–493. https://doi.org/10.1002/hipo.20914.
Scharfman, H.E., Goodman, J.H., Sollas, A.L., 2000. Granule-like neurons at the hilar/CA3 border after status epilepticus and their synchrony with area CA3 pyramidal cells: functional implications of seizure-induced neurogenesis. J. Neurosci. 20, 6144–6158. https://doi.org/10.1523/JNEUROSCI.20-16-06144.2000.
Scharfman, H.E., Sollas, A.E., Berger, R.E., Goodman, J.H., Pierce, J.P., 2003. Perforant path activation of ectopic granule cells that are born after pilocarpine-induced seizures. Neuroscience 121, 1017–1029. https://doi.org/10.1016/s0306-4522(03)00481-0.
Schnizler, M.K., Schnizler, K., Zha, X.-M., Hall, D.D., Wemmie, J.A., Hell, J.W., Welsh, M. J., 2009. The cytoskeletal protein alpha-actinin regulates acid-sensing ion channel 1a through a C-terminal interaction. J. Biol. Chem. 284, 2697–2705. https://doi.org/10.1074/jbc.M805110200.
Seinfeld, J., Baudry, N., Xu, X., Bi, X., Baudry, M., 2016. Differential Activation of Calpain-1 and Calpain-2 following Kainate-Induced Seizure Activity in Rats and Mice. eNeuro 3. https://doi.org/10.1523/ENEURO.0088-15.2016.
Sekino, Y., Kojima, N., Shirao, T., 2007. Role of actin cytoskeleton in dendritic spine morphogenesis. Neurochem. Int. 51, 92–104. https://doi.org/10.1016/j.neuint.2007.04.029.
Selliah, N., Brooks, W.H., Roszman, T.L., 1996. Proteolytic cleavage of alpha-actinin by calpain in T cells stimulated with anti-CD3 monoclonal antibody. J. Immunol. Baltim. Md 1950 (156), 3215–3221.
Seress, L., Pokorny, J., 1981. Structure of the granular layer of the rat dentate gyrus. A light microscopic and Golgi study. J. Anat. 133, 181–195.
Shao, H., Wang, J.H.-C., Pollak, M.R., Wells, A., 2010. α-actinin-4 is essential for maintaining the spreading, motility and contractility of fibroblasts. PLoS One 5, e13921. https://doi.org/10.1371/journal.pone.0013921.
Shao, H., Li, S., Watkins, S.C., Wells, A., 2014. α-Actinin-4 is required for amoeboid-type invasiveness of melanoma cells. J. Biol. Chem. 289, 32717–32728. https://doi.org/10.1074/jbc.M114.579185.
Sharvit, E., Abramovitch, S., Reif, S., Bruck, R., 2013. Amplified inhibition of stellate cell activation pathways by PPAR-γ, RAR and RXR agonists. PLoS One 8, e76541. https://doi.org/10.1371/journal.pone.0076541 eCollection 2013.
Sjöblom, B., Salmazo, A., Djinović-Carugo, K., 2008. Alpha-actinin structure and regulation. Cell. Mol. Life Sci. CMLS 65, 2688–2701. https://doi.org/10.1007/s00018-008-8080-8.
Sloviter, R.S., 1987. Decreased hippocampal inhibition and a selective loss of interneurons in experimental epilepsy. Science 235, 73–76. https://doi.org/10.1126/science.2879352.
Sloviter, R.S., Zappone, C.A., Bumanglag, A.V., Norwood, B.A., Kudrimoti, H., 2007. On the relevance of prolonged convulsive status epilepticus in animals to the etiology and neurobiology of human temporal lobe epilepsy. Epilepsia 48 (Suppl. 8), 6–10. https://doi.org/10.1111/j.1528-1167.2007.01335.x.
Small, J.V., Stradal, T., Vignal, E., Rottner, K., 2002. The lamellipodium: where motility begins. Trends Cell Biol. 12, 112–120. https://doi.org/10.1016/s0962-8924(01)02237-1.
Soria Fregozo, C., Pérez Vega, M.I., 2012. Actin-binding proteins and signalling pathways associated with the formation and maintenance of dendritic spines. Neurologia. 27, 421–431. https://doi.org/10.1016/j.nrl.2011.10.005.
Soussi, R., Boulland, J.-L., Bassot, E., Bras, H., Coulon, P., Chaudhry, F.A., Storm-Mathisen, J., Ferhat, L., Esclapez, M., 2015. Reorganization of supramammillary-

hippocampal pathways in the rat pilocarpine model of temporal lobe epilepsy: evidence for axon terminal sprouting. Brain Struct. Funct. 220, 2449–2468. https://doi.org/10.1007/s00429-014-0800-2.

Troy, C.M., Friedman, J.E., Friedman, W.J., 2002. Mechanisms of p75-mediated death of hippocampal neurons. Role of caspases. J. Biol. Chem. 277, 34295–34302. https://doi.org/10.1074/jbc.M205167200.

Tseng, P.Y., Henderson, P.B., Hergarden, A.C., Patriarchi, T., Coleman, A.M., Lillya, M. W., Montagut-Bordas, C., Lee, B., Hell, J.W., Horne, M.C., 2017. α-Actinin Promotes Surface Localization and Current Density of the $Ca^{2+}$ Channel $Ca_V1.2$ by Binding to the IQ Region of the α1 Subunit. Biochemistry. 56, 3669–3681. https://doi.org/10.1021/acs.biochem.7b00359.

Walikonis, R.S., Jensen, O.N., Mann, M., Provance, D.W., Mercer, J.A., Kennedy, M.B., 2000. Identification of proteins in the postsynaptic density fraction by mass spectrometry. J. Neurosci. 20, 4069–4080. https://doi.org/10.1523/JNEUROSCI.20-11-04069.2000.

Walikonis, R.S., Oguni, A., Khorosheva, E.M., Jeng, C.J., Asuncion, F.J., Kennedy, M.B., 2001. Densin-180 forms a ternary complex with the (alpha)-subunit of Ca2+/calmodulin-dependent protein kinase II and (alpha)-actinin. J. Neurosci. 21, 423–433. https://doi.org/10.1523/JNEUROSCI.21-02-00423.2001.

Worth, D.C., Daly, C.N., Geraldo, S., Oozeer, F., Gordon-Weeks, P.R., 2013. Drebrin contains a cryptic F-actin–bundling activity regulated by Cdk5 phosphorylation. J. Cell Biol. 202, 793–806. https://doi.org/10.1083/jcb.201303005.

Wyszynski, M., Lin, J., Rao, A., Nigh, E., Beggs, A.H., Craig, A.M., Sheng, M., 1997. Competitive binding of alpha-actinin and calmodulin to the NMDA receptor. Nature 385, 439–442. https://doi.org/10.1038/385439a0.

Wyszynski, M., Kharazia, V., Shanghvi, R., Rao, A., Beggs, A.H., Craig, A.M., Weinberg, R., Sheng, M., 1998. Differential regional expression and ultrastructural localization of alpha-actinin-2, a putative NMDA receptor-anchoring protein, in rat brain. J. Neurosci. 18, 1383–1392. https://doi.org/10.1523/JNEUROSCI.18-04-01383.1998.

Yahara, I., Harada, F., Sekita, S., Yoshihira, K., Natori, S., 1982. Correlation between effects of 24 different cytochalasins on cellular structures and cellular events and those on actin in vitro. J. Cell Biol. 92, 69–78. https://doi.org/10.1083/jcb.92.1.69.

Zubareva, O.E., Kovalenko, A.A., Kalemenev, S.V., Schwarz, A.P., Karyakin, V.B., Zaitsev, A.V., 2018. Alterations in mRNA expression of glutamate receptor subunits and excitatory amino acid transporters following pilocarpine-induced seizures in rats. Neurosci. Lett. 686, 94–100. https://doi.org/10.1016/j.neulet.2018.08.047.